

General Disclaimer

One or more of the Following Statements may affect this Document

- This document has been reproduced from the best copy furnished by the organizational source. It is being released in the interest of making available as much information as possible.
- This document may contain data, which exceeds the sheet parameters. It was furnished in this condition by the organizational source and is the best copy available.
- This document may contain tone-on-tone or color graphs, charts and/or pictures, which have been reproduced in black and white.
- This document is paginated as submitted by the original source.
- Portions of this document are not fully legible due to the historical nature of some of the material. However, it is the best reproduction available from the original submission.

Research Study of Droplet Sizing Technology
Leading to the Development of an Advanced
Droplet Sizing System

C.F. Hess, A.E. Smart, and V.E. Espinosa

Spectron Development Laboratories, Inc.
Costa Mesa, California

(NASA-CR-174839) RESEARCH STUDY OF DROPLET
SIZING TECHNOLOGY LEADING TO THE DEVELOPMENT
OF AN ADVANCED DROPLET SIZING SYSTEM Final
Report (Spectron Development Labs., Inc.)
88 p AC A05/MF 101

N85-21604

Unclas
14187

CSCI 14B G3/35

January 1985



Prepared for

NATIONAL AERONAUTICS AND SPACE ADMINISTRATION
Lewis Research Center
Under Contract NAS 3-23538

TABLE OF CONTENTS

<u>NO.</u>		<u>PAGE</u>
1.0	INTRODUCTION.....	1
2.0	ASSOCIATED RESEARCH.....	3
2.1	Research Associated with the Visibility/ Intensity Technique.....	3
2.2	Research Associated with the IMAX Technique.....	5
3.0	THE VISIBILITY/INTENSITY TECHNIQUE.....	6
3.1	Errors in the Visibility Measurements.....	6
3.2	Description of the V/I Technique.....	7
3.3	Results Obtained with the V/I Technique.....	11
3.4	The V/I Probe Volume.....	20
3.5	Simplified Probe Volume	21
4.0	THE IMAX TECHNIQUE.....	31
4.1	Two-Color System.....	32
4.2	Single Color System.....	41
4.3	A Self-Calibrating Algorithm Combining IMAX with V/I.....	46
4.4	The IMAX Probe Volume.....	47
4.5	Description of IMAX Breadboard.....	52
4.6	Results Obtained with the IMAX Technique.....	52
5.0	THE ADVANCED DROPLET SIZING SYSTEM (ADSS).....	64
5.1	Operating Ranges and Specifications.....	71
6.0	TRANSMITTER.....	72
6.1	Transmitter Description.....	72
7.0	RECEIVER.....	76
7.1	Receiver Description.....	76
8.0	V-I/IMAX INTERFACE BOX.....	79
8.1	High Voltage Control.....	79
8.2	Intensity Measurement.....	81
8.2.1	Overview.....	81
9.0	PUBLICATIONS.....	84
10.0	REFERENCES.....	85

1.0 INTRODUCTION

This report summarizes the work conducted by Spectron Development Laboratories (SDL) for the Combustion Fundamentals Group of NASA Lewis. The work was performed in three phases over the time period 24 September 1982 through 30 July 1984. The first phase consisted of a comprehensive laboratory assessment and evaluation of two defined optical techniques for particle characterization. These techniques are Visibility/Intensity (V/I) and Maximum Scattered Intensity (IMAX). The first (V/I) was proposed as an improvement to the problems found with the visibility technique. The second (IMAX) is an innovative technique which uses a pulse height analyzer combined with LDV to measure the size and velocity of droplets in a spray.

The second phase of this effort was to upgrade the Droplet Sizing System of NASA Lewis using the newly researched technologies. This phase was, however, substituted by a Phase 3 which consisted of developing completely new optical transmitter and receiver which would make use of either V/I or IMAX in the determination of droplet size and velocity. The decision to incorporate both techniques into the instrument was made when there were not sufficient facts to indicate the superiority of one technique over the other. The facts a posteriori show that IMAX is a more powerful technique with the potential of expanding the dynamic size range to about 30:1 and to perform measurements with more accuracy.

This document is structured to report the work conducted under all the phases.

First, an overview of related work by other researchers is given; a description is then given of the various techniques studied

under this contract, and along with each technique a sample of meaningful results is provided. It should be pointed out that the "main techniques" are V/I and IMAX but the latter is further subdivided into the two-color and single-color systems.

The report is completed with a description of the system developed, built, and delivered to NASA. We would also like to acknowledge that a large portion of the support for the R and D phase has come from the Air Force Office of Scientific Research under Contract No. F49620-83-C-0060. Finally, it should be apparent to the reader that although this report summarizes the entire work, the final product of Phase 3 is a sophisticated instrument consisting of optics, electronics, computer software, and the documentation necessary to operate it.

2.0 ASSOCIATED RESEARCH

2.1 Research Associated with the Visibility/Intensity Technique

The interferometric technique to measure the size and velocity of particles flowing in a fluid has been in existence for approximately one decade. Farmer¹ introduced the concept of using visibility for particle sizing in the forward scattering direction. Since then, many researchers have contributed to the development of the technique. Robinson and Chu², for instance, rederived Farmer's results using a more rigorous approach, and the definition of visibility through the first order Bessel function was confirmed experimentally in forward scatter. However, contrary to what was thought at the time, this visibility relationship could not be used at any angle other than the forward or zero degree. Adrian and Orloff³ showed that it could not be used in the backscatter mode as predicted by Mie scattering theory. This finding was also confirmed by Roberds⁴, who in addition showed that the configuration of the receiving optics would also affect the relationship between visibility and size.

The biggest known limitation of the visibility technique was its inability to measure particles in a dense field. The main reason being that the probe volume when observed in the forward direction is big and, therefore, the criterion of single particle measurement is not always met. In addition, the technique dictated that the largest measurable droplet was of the order of the fringe spacing. This imposes a limitation of about 200 μm to the largest measurable particle and also results in a large probe volume, since a minimum number of fringes is needed (typically 8) to accurately process a Doppler signal.

Bachalo⁵ formulated a mathematical model based on classical optics where the Mie scattering is approximated with refraction, diffraction and reflection. That model was used to predict the visibility of spherical particles in off-axis directions. Experimental results using monodispersed droplets confirmed the validity of the model under many conditions. Pendleton⁶ later confirmed these results using a sophisticated numerical model that utilizes the full Mie equations. Recent work conducted under this contract at SDL shows that there are two major limitations on the existing models. First, all the theories developed thus far predict the Mie scattering from beams of uniform intensity. Second, the formation of the fringe pattern at the probe volume may be affected by secondary scattering of particles immersed in the laser beams before they cross. As a result of these limitations, the relationship between visibility and size is not straight forward and considerable errors can be made. A model proposed by M.L. Yeoman et al⁷ pursues the solutions of the above problems. It consists of two concentric interferometric patterns of two colors such that the small one establishes a region of the big one where the hyperbolic variation of the visibility is negligible. Also digital analysis of the signals helps establish some that are in error. The results reported here show that using the intensity of the pedestal of the scattered light in addition to the visibility will eliminate many of these errors, significantly improving measurement accuracy.

2.2 Research Associated with the IMAX Technique

Several nonintrusive single particle counters (NSPCs) using absolute scattered light have been proposed and they can be divided into two groups. In the first group⁽⁸⁻¹⁰⁾ Gaussian laser beams are used and various mathematical inversion techniques have been proposed to extract the true size distribution from the signal amplitude distribution. Several assumptions are needed to perform such inversion, such as assuming the form of the size distribution⁽⁸⁾ or a uniform average velocity for all the particles regardless of size⁽⁹⁾. A method to account for pinhole masking has also been described⁽¹⁰⁾. The second group of NSPC's uses a probe volume of known illumination to avoid the ambiguity of particle position. The technique described here falls in this group. Several approaches have been proposed^(7,11,12,13) to accomplish this task. Apertures are used to cut off the edges of the Gaussian beam and thus image a probe volume of almost uniform illumination^(11,12). One of the apertures⁽¹¹⁾ had, in addition, two wedges that, when properly oriented, can be used to obtain the velocity vector in two components (magnitude and direction). Ring-shaped probe volumes have also been produced⁽¹³⁾ by a TEM₀₁ laser and a ring-shaped aperture. The measurement volume is defined by the intersection of apertures in front of two photomultipliers.

3.0 THE VISIBILITY/INTENSITY TECHNIQUE

In this section a description is given of some of the problems associated with the visibility technique, and how many of these problems can be corrected or avoided combining the visibility with the intensity of the scattered light.

3.1 Errors in the Visibility Measurements

The prediction of the droplet size based on the visibility of the light scattered by the droplet crossing an interferometric pattern of fringes is dependent on the pattern itself. For a perfect system the fringe visibility should be 100% and the light scattered should be primarily of one type. There are, however, many reasons in practical environments that contribute to alter the fringe pattern and, therefore, confuse the relationship between visibility and size. The result is that apparent sizes instead of true sizes are often measured. As an example, droplets interacting with the laser beams before they cross will randomly reduce (or even destroy) the fringe visibility. If a droplet is measured at such time, it will appear bigger than its true size. There are several factors that produce an error in the visibility measurement and they are listed below. They are divided into two groups: the ones that reduce the visibility and the ones that increase it.

A) Factors that Reduce the Visibility

- 1) Particles prior to crossover destroy fringe contrast. This is a function of the spray density.
- 2) Beam excursions due to turbulent hot media.
- 3) Hyperboloidal reduction of visibility.

- 4) Reflection/refraction can add destructively for large droplets immersed in a nonuniform (typically Gaussian) beam.
- 5) Multiple particles in probe volume.
- 6) Increase in signal background. Normally from many little drops present in the probe volume.
- 7) Loss of fringe contrast due to faulty components (beam splitter, etc.).

B) Factors that Increase the Visibility

- 1) Out of focus drops "masked" by the pinhole.
- 2) Low level signals in the presence of a noisy background.
- 3) High time rise on leading edge of signal.

3.2 Description of the V/I Technique

This technique makes use not only of the visibility of the signal but also the peak intensity of the pedestal. Both parameters are available in the signal and their cross-correlation can be used to eliminate faulty signals produced in many practical environments. This technique will especially prevent small particles (high visibility) from appearing as large. Figure 3.1 shows a Doppler trace where both the visibility and the peak intensity of the pedestal are defined. There is a correlation between the size of the droplet and the amount of scattered light given by Mie theory. This correlation can be used to eliminate signals with an apparently different size. The proposed logic is as follows: droplets that produce a certain visibility must have a given size; hence, they must scatter light with a given intensity (characterized by I_p). Two exceptions are contemplated: first, droplets with the correct

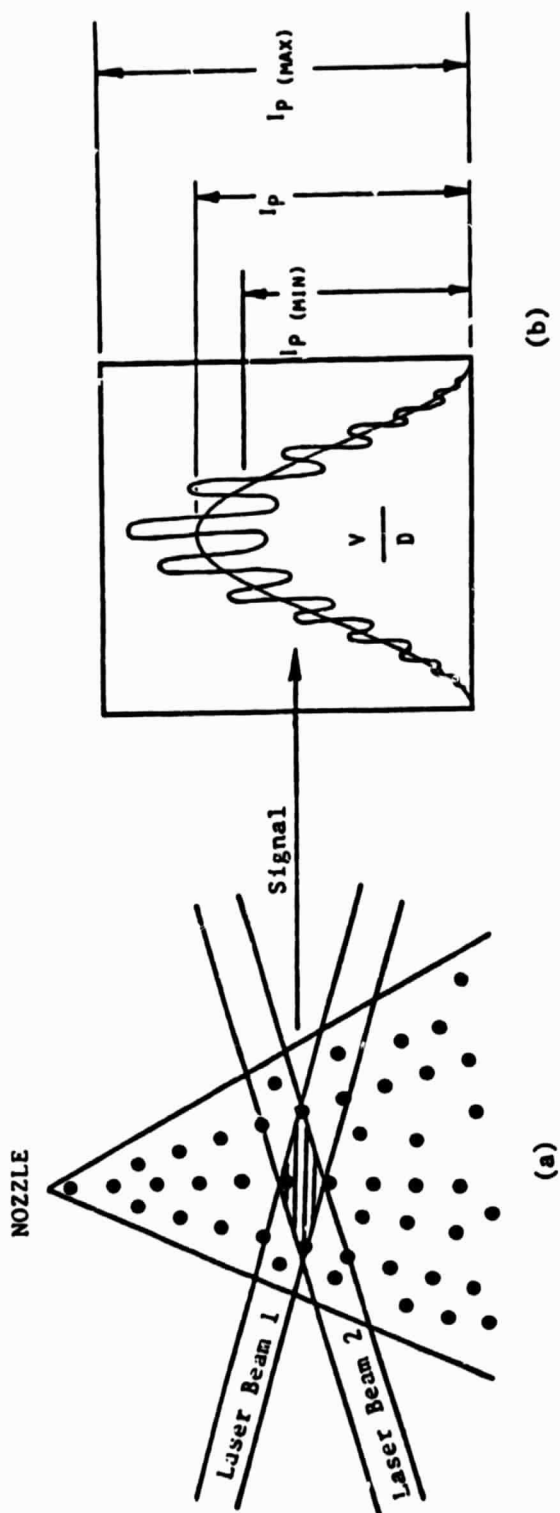


Figure 3.1. Schematic Representation of Doppler Burst Used in the Visibility/Intensity Technique. D is the droplet diameter, V its visibility, I_p the peak pedestal intensity, and $I_p (\text{min})$ and $I_p (\text{max})$ arbitrary limits of acceptability of I_p .

visibility will scatter different amounts of light due to the Gaussian nature of the probe volume's intensity; second, droplets with an erroneous visibility will not scatter light with an intensity corresponding to their apparent size.

The V/I method will then establish intensity limits for every measured visibility. This will produce a well established probe volume as a function of size and will reject droplets measured with an erroneous visibility. For instance, assume that the size corresponding to a visibility V_1 is d_1 . Then the light scattered will have a pedestal with maximum intensity $I_{p_1}(\text{max})$. Since this intensity would only be detected from droplets crossing through the middle of the probe volume, more relaxing limits are proposed. That is I_{p_1} will be accepted when $I_{p_1}(\text{min}) < I_{p_1} < I_{p_1}(\text{max})$. Obviously, the broader the limits, the larger the error that can be allowed with the visibility technique.

Figure 3.2 shows three cases that illustrate the correcting properties of the V/I method. Figure 3.2a shows a droplet of size d_1 with visibility V_1 and intensity I_{p_1} . Since this last one is within established limits, the signal is accepted as valid. Figure 3.2b shows the signal produced by a droplet of diameter d_2 but the visibility was reduced to V_1 due to fringe contrast reduction. Since the visibility is V_1 , this signal would be interpreted as having a diameter d_1 . However, the peak intensity of the pedestal I_{p_2} corresponds to its true size (d_2) and is smaller than $I_{p_1}(\text{min})$ (to which it is compared) and hence, the signal is rejected. Figure 3.2c shows the signal of another droplet of diameter d_2 but with correct visibility V_2 and corresponding pedestal I_{p_2} . This last one will also be accepted.

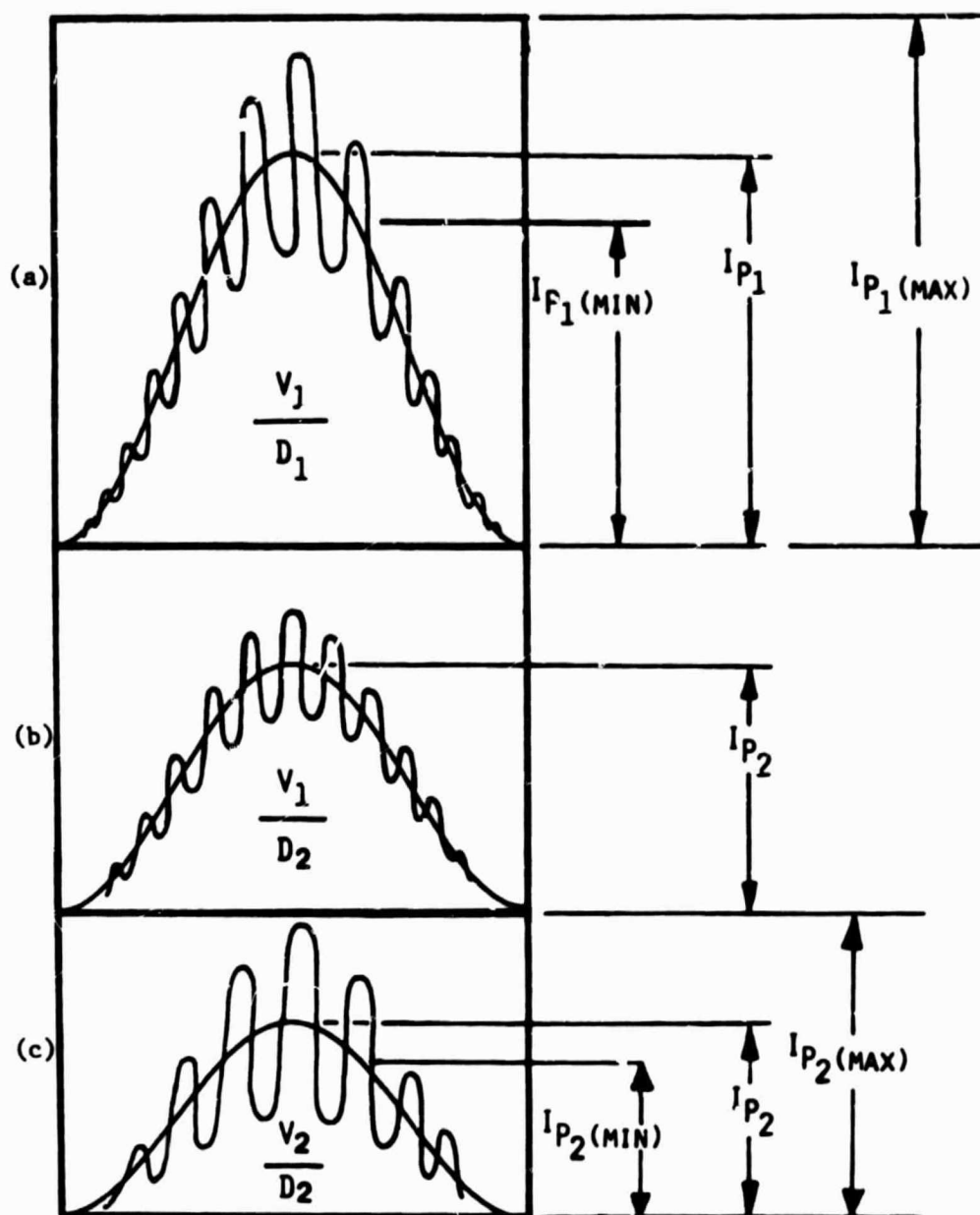


Figure 3.2. Visibility and Intensity of Two Size Droplets.

(a) and (c) correspond to droplets traveling through the middle of an undisturbed probe volume; (b) could be from a small droplet traveling thru the middle of a disturbed probe volume or a large droplet traveling through the edge of the Gaussian probe volume.

Since the intensity limits are functions of droplet size, a variable filter like the one shown on Figure 3.3 is necessary. It contains the intensity limits $I_p(\min)$, $I_p(\max)$ corresponding to any visibility (V). Figures 3.4a and 3.4b show the raw data and software filtered data in an intensity/visibility plot. Figure 3.4a shows that the intensity is bounded by $I_p(\max)$ (with a few exceptions due to light re-radiated by upstream droplets). Points with different intensity/visibility combinations can be either due to droplets moving through the tail of the Gaussian intensity profile of the probe volume or to droplets with an erroneous visibility. By limiting the intensity of the pedestal for which a signal is considered valid, two things are accomplished: (1) the limits of the probe volume are carefully established; and, (2) most importantly, most of the signals with erroneous visibility are rejected.

3.3 Results Obtained with the V/I Technique

Experimental results are presented to illustrate the accuracy and resolution of the visibility/intensity technique, and how it compares with visibility only.

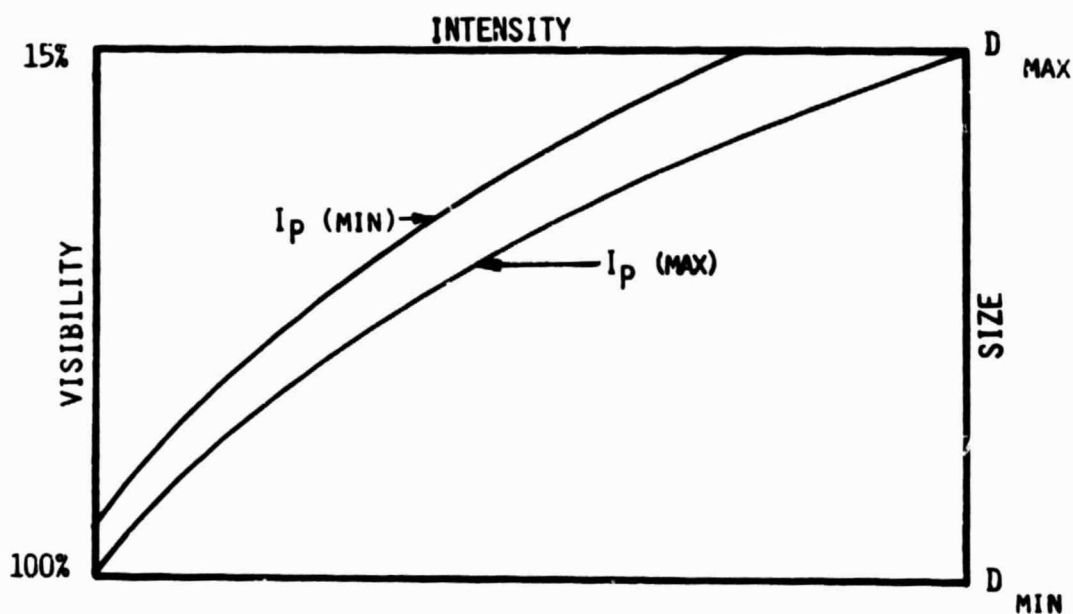
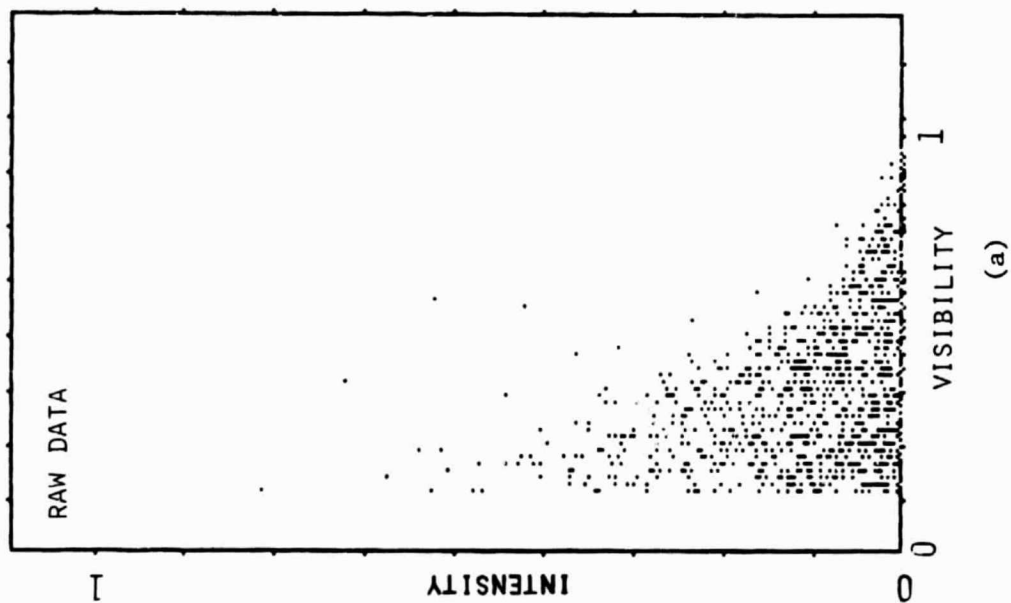
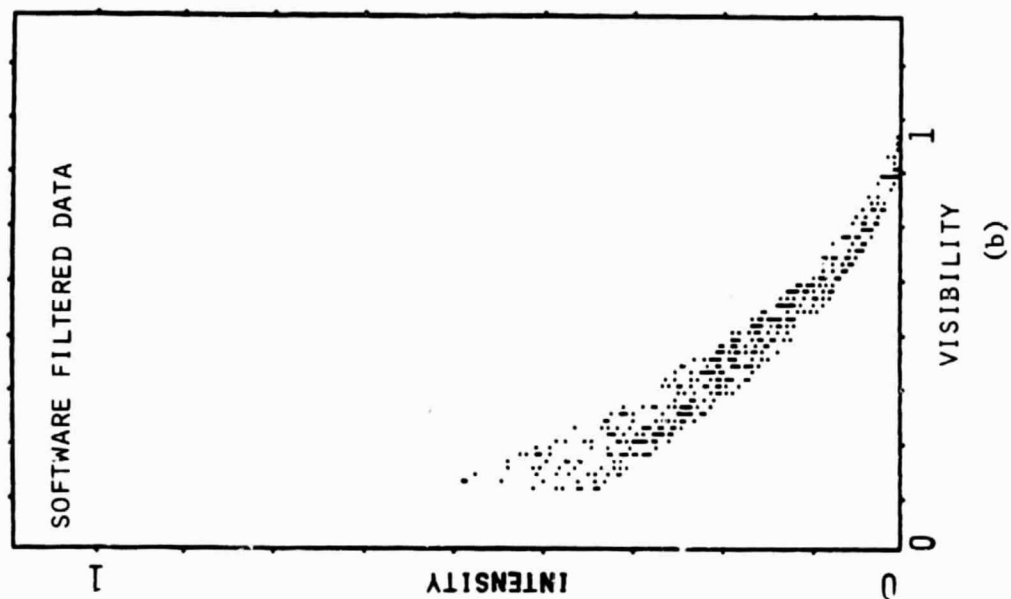


Figure 3.3. Variable Intensity vs. Visibility Software Filter



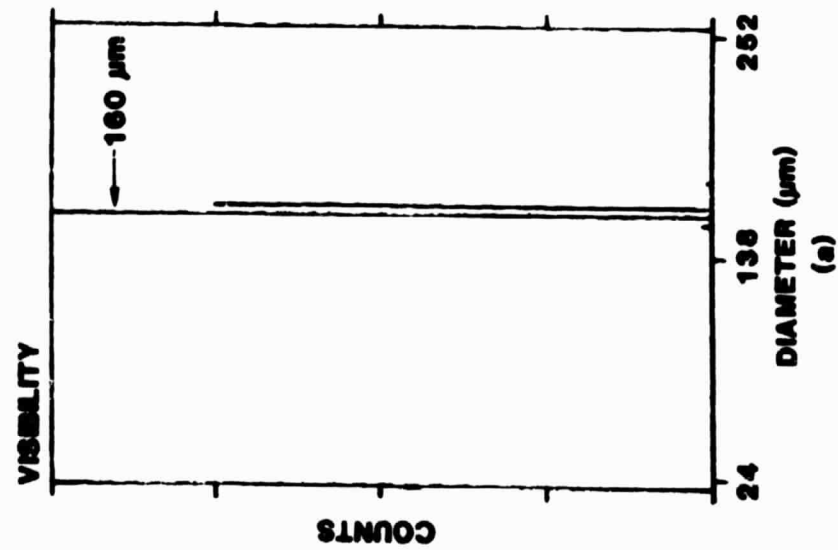
Unfiltered visibility vs. Intensity
data of droplets in a spray



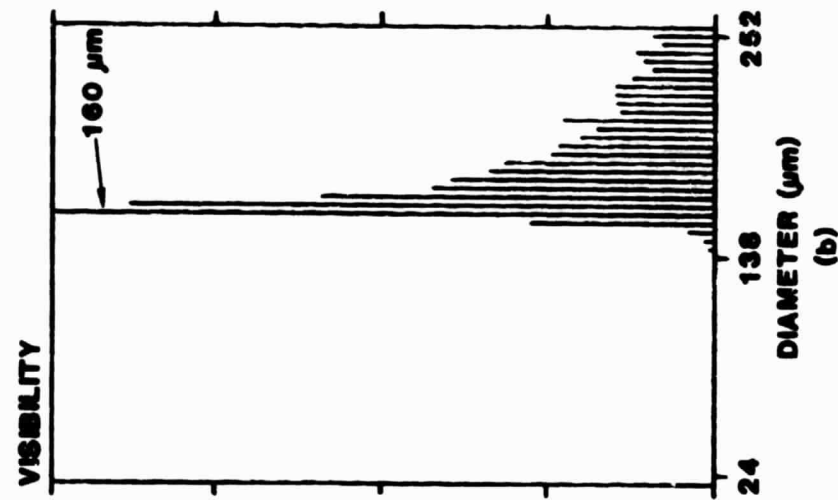
Software filtered data of Figure 3.4 a

Figure 3.4. Preliminary Results of Visibility/Intensity Assessment

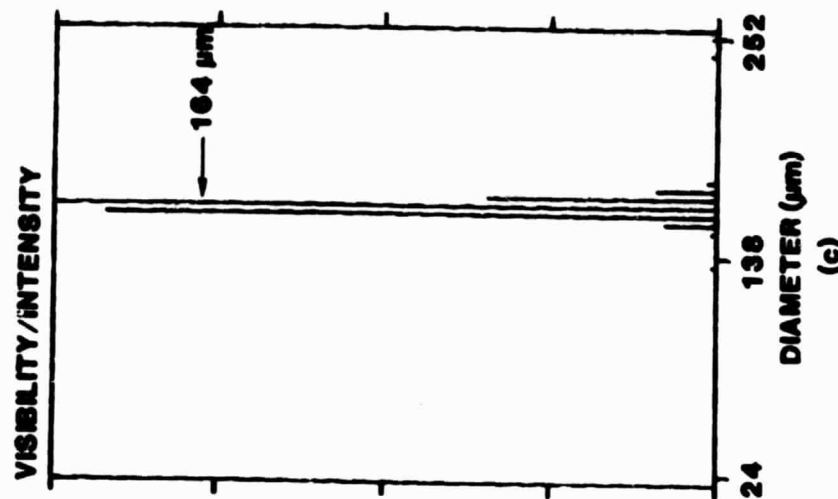
MONODISPersed DROPLETS



**MONODISPersed DROPLETS
WITH SPRAY BLOCKING BEAMS**



**MONODISPersed DROPLETS
WITH SPRAY BLOCKING BEAMS**



FRINGE SPACE: 37 μm

f No. = 5

θ = 30°

Figure 3.5. Size Distribution of a Monodispersed String of Droplets

- (a) Monodisperse Droplets Measured with V/I, No Spray Blockage
- (b) Monodisperse Droplets Measured with Visibility Only.
Blocking Spray Before Crossover.
- (c) Monodisperse Droplets Measured with V/I. Blocking
Spray Before Crossover.

Effect of Beam Blockage on Size Distribution

The effect of a very dense spray blocking the laser beams before the probe volume was studied. Figure 3.5a shows the histogram produced when monodispersed droplets travel through the middle of an undisturbed probe volume. Figure 3.5b shows a histogram obtained with the visibility technique of the same monodispersed droplets but now the laser beams have traveled through a real spray before crossing. We made sure that the spray was not going into the probe volume. The fringe pattern produced by crossing two laser beams is well behaved and theoretically predicted in the undisturbed case. However, when the beams travel through a spray, this fringe pattern can be considerably altered due to random beam blockage. The result can be a distorted Doppler signal with a visibility, both lower and higher than that predicted theoretically. Considerable error in the size distribution will then be observed. The size of the error depends on the visibility itself. It is quite apparent from the histograms that what should be a monodispersed distribution is measured as a very broad one. The next histogram shown on Figure 3.5c shows the results obtained with V/I when the beams travel through the spray before crossing (same conditions as Figure 3.5b). Notice that a very narrow distribution is thus obtained.

V/I Measurements with the Berglund-Liu Droplet Generator

The calibration and verification source used in these experiments was the Berglund Liu monodisperse droplet generator. This generator can work in two modes: (a) it can generate a string of droplets of known size and equally spaced at the measurement point; (b) using a cap and

dispersion air, these droplets can be dispersed into a spray of monodispersed droplets.

It has been observed in previous studies¹⁴ that under some dispersion air conditions, some of the droplets will collide and form other droplets with double or even triple the volume. Therefore, if the primary droplet diameter is d_0 , then droplets with diameter $2^{1/3}d_0$ and $3^{1/3}d_0$ can be produced. It must be pointed out that in these studies, we did not obtain photographic measurements to verify the presence of the secondary droplets. The size of the primary droplets was accurately predicted from the flow rate and frequency of vibration of the pinhole.

One limitation imposed by the Berglund Liu is that it cannot produce droplets of a given size at arbitrary spacing. Since the measurement instrument requires the presence of only one droplet in the probe volume, that limits the size droplet that can be measured.

The procedure used in these experiments was to produce a string of large monodispersed droplets to calibrate the instrument. Then smaller droplets were produced by increasing the frequency of vibration of the orifice, and with the dispersion air a spray of these droplets was formed. Typical number density at the probe volume was 500 droplets/cc, and the diameter of the spray at the plane of measurements was about 4 mm.

A DSI system with V/I capability was used to obtain the data shown below.

Optical configuration:

- Collection angle of 30°
- Transmitting lens = 495 mm
- Waist diameter = 300 μm
- Fringe spacing = 13.6 μm
- Collection F# = 5

The high voltage to the photomultiplier was established with a droplet string of diameter 100 μm .

The size range of interest was 9 to 92 μm .

A spray of droplets with primary diameter of 53 μm was then produced using the Berglund Liu with a flow rate of 0.21 cc/min and frequency of 45.8K Hz and the dispersion air. For the conditions selected above, this size will produce a visibility of 58%.

Notice that for primary droplets of 53 μm , the doublets will have a diameter of $2^{1/3} \times 53 = 66 \mu\text{m}$, and the triplets' diameter will be $3^{1/3} \times 53 = 76 \mu\text{m}$.

Results are shown for both visibility/intensity and visibility only to provide some comparison.

Figure 3.6 shows the measurements of the monodispersed spray of 53 μm .

Figure 3.7a shows the data of the spray formed of primary droplets and doublets.

Figure 3.7b shows results similar to Figure 3.7a but obtained with visibility only. Notice how much broader the distributions are.

Figure 3.7c shows a spray containing primary droplets, doublets and triplets.

Figure 3.7d shows results similar to Figure 3.7c but obtained with visibility only. Notice that the distribution is broader and the resolution is not as fine.

Both the accuracy and resolution of these measurements are very good. The theoretically predicted sizes are $53\text{ }\mu\text{m}$, $66\text{ }\mu\text{m}$, and $76\text{ }\mu\text{m}$. The corresponding measured diameters are (52 to 54), (63 to 65), and $73\text{ }\mu\text{m}$.

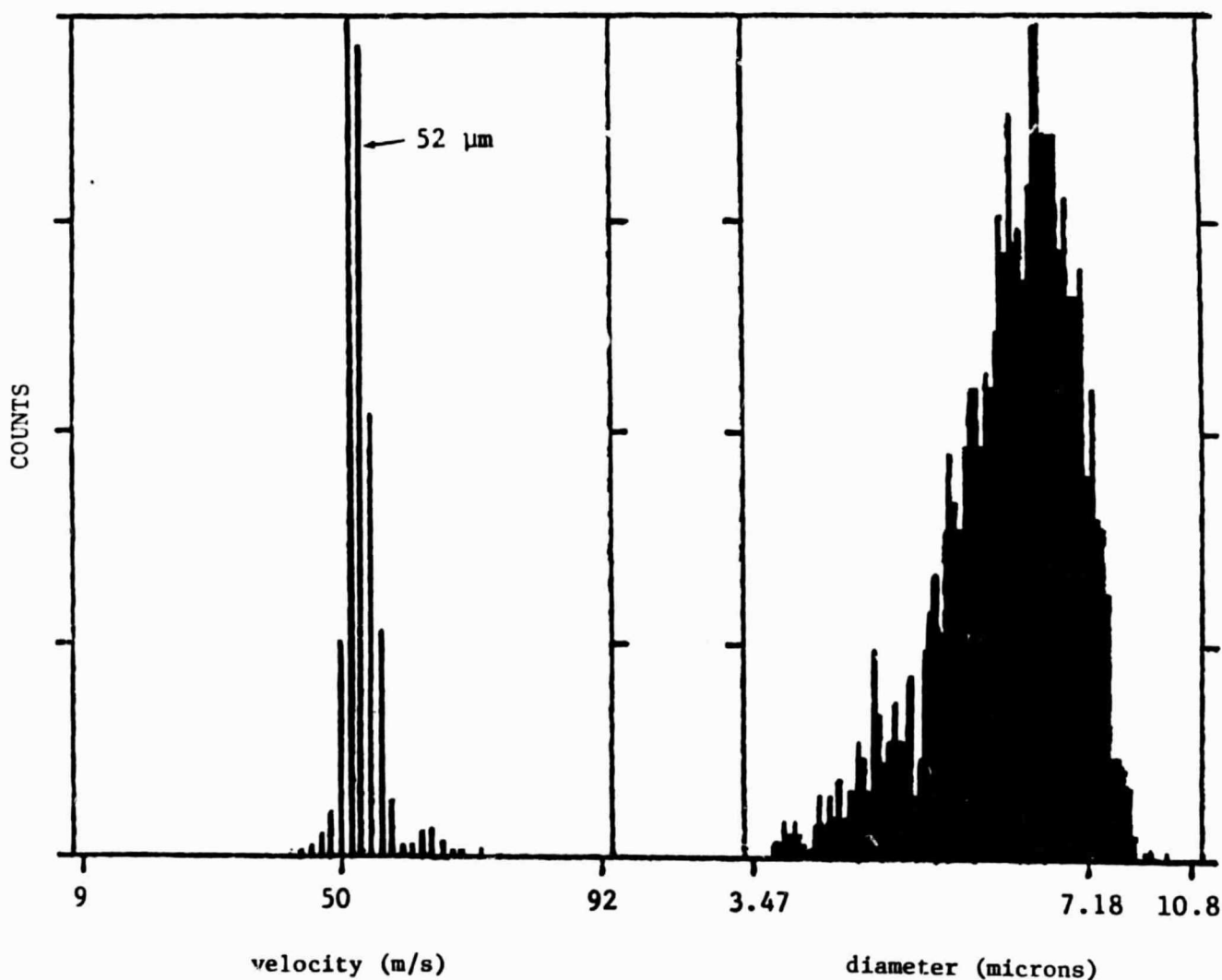


FIGURE 3.6

VISIBILITY/INTENSITY MEASUREMENTS OF MONODISPERSED SPRAY

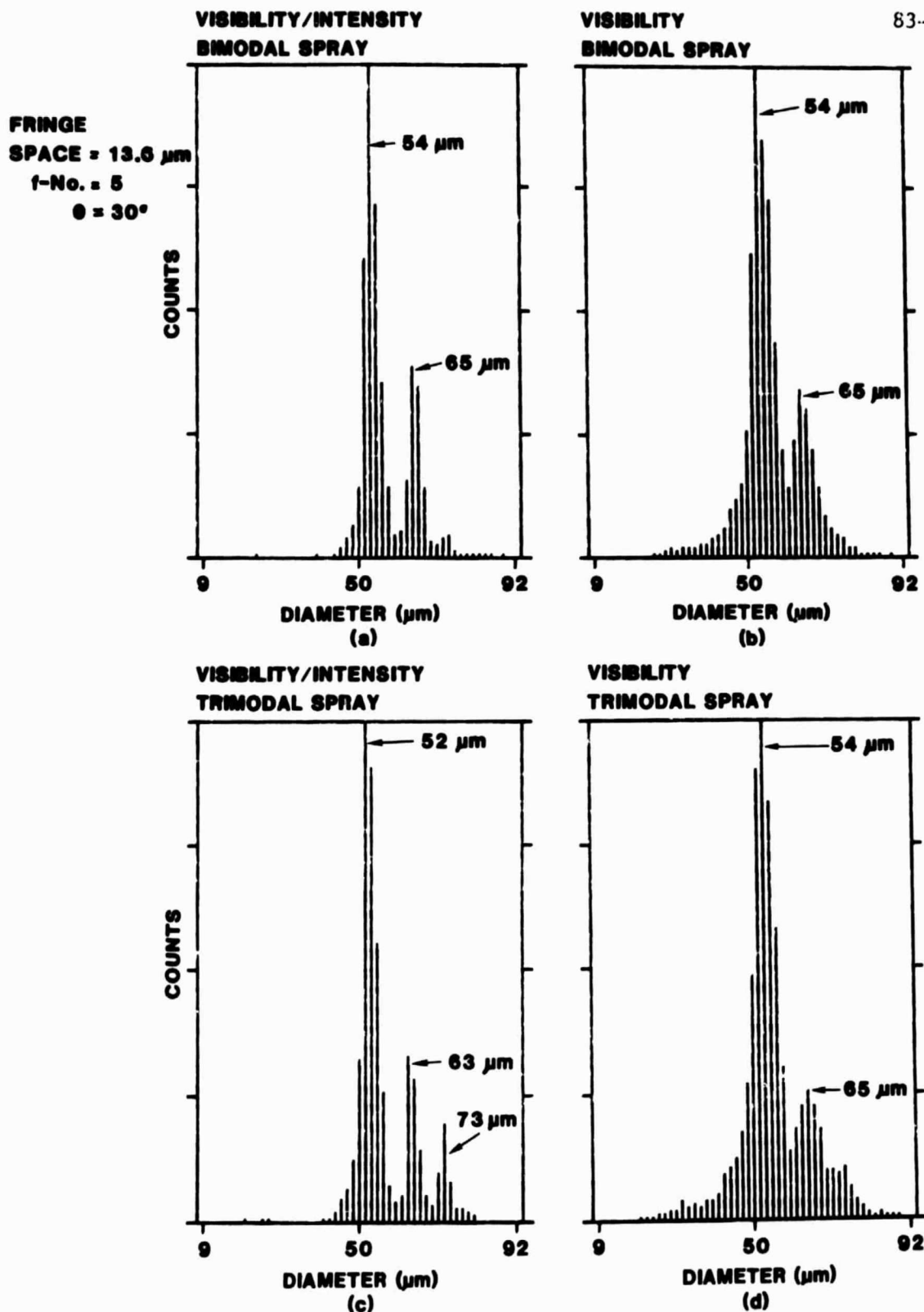


Figure 3.7. Size Distributions of Bimodal and Trimodal Sprays with Visibility/Intensity

3.4 The V/I Probe Volume

An important aspect of any optical technique is the recognition and determination of the probe volume. The implication is that different size particles scatter different amounts of light (typically proportional to the square of the diameter). Also, the intensity of the probe volume is non-uniform (typically Gaussian). Therefore, for a given threshold level the volume of detectability is a function of particle size. This will introduce a natural bias in the histogram of particle size. To correct this bias the probe volume needs to be computed as a function of particle size and optical configuration and then used to correct the biased histogram.

A : area of measuring region
b₀ : waist radius
CF : collection factor
D_p : diameter of pinhole
D_{laser} : diameter of laser
d : diameter of droplet
d₀ : maximum droplet diameter ($d_0/\delta CF = .845$) for a given size range
f : focal length of transmitting lens
f₁ : focal length of 1st collecting lens
f₂ : focal length of 2nd collecting lens
I_{Th} : ground to peak threshold (front panel in volts)
I_s : d_c saturation (0.65 volts)
N : fringes required by processor (front panel)
P : pedestal intensity
V : visibility of size d
V₀ : visibility of size d₀ (V₀ = .151)
x : coordinate normal to fringes

y, z : coordinates
 δ : fringe spacing
 γ : crossover angle
 θ : angle of collection

3.5 Simplified Probe Volume Model

The cross-sectional area is given by:

$$A = \frac{2D_p y}{\sin \theta} \cdot \frac{f_1}{f_2} \quad (1)$$

where y must be calculated based on the Gaussian profile and d (droplet diameter).

Let us call I_g the saturation level imposed by the electronics.

Then for the largest detectable droplet:

$$I_{\text{peak}} < I_g.$$

The intensity profile of a probe volume formed by crossing two Gaussian beams is given by:

$$I = 2I_o \exp \left\{ \left(\frac{-2}{b_o^2} \right) \left[x^2 + y^2 + \frac{z^2 \gamma^2}{4} \right] \right\} \left[\cos h \left(\frac{2 x z \gamma}{b_o^2} \right) + \cos \frac{4\pi x \sin \left(\frac{\gamma}{2} \right)}{\lambda} \right] .$$

For a pinhole limited signal, we can assume z to be small; therefore,

$$I = 2I_0 \exp \left[\left(\frac{-2}{b_0^2} \right) (x^2 + y^2) \right] \cdot \left[1 + \cos \frac{2\pi y x}{\lambda} \right] .$$

The pedestal scattered by the droplet of diameter d is given by:

$$P = 2I_0 K_0 d^2 \exp \left[\left(\frac{-2}{b_0^2} \right) (x^2 + y^2) \right] .$$

The intensity scattered by the same droplet is given by:

$$I_s = 2I_0 K_0 d^2 \exp \left[\left(\frac{-2}{b_0^2} \right) (x^2 + y^2) \right] \left[1 + \frac{\cos 2\pi y x}{\lambda} \cdot v \right] \quad (2)$$

The peak intensity occurs at $x=0, y=0$; and for the largest droplet, it is given by:

$$I_{\text{peak}} = 2I_0 K_0 d_c^2 (1 + v_0) < I_s .$$

Solving for I_0 :

$$I_o = \frac{I_s}{2K_o d_o^2 (1 + v_o)} \quad . \quad (3)$$

The expression for the peak-to-peak intensity I_{ac} can be obtained by setting the cosine term to +1 and -1 in Equation 2, and then subtracting:

$$\therefore I_{ac} = 4I_o K_o v d_o^2 \exp \left[\left(\frac{-2}{b_o} \right) (x^2 + y^2) \right] \quad .$$

Substituting Equation 3 in the above equation, we get:

$$I_{ac} = \frac{2d^2 v I_s}{d_o^2 (1 + v_o)} \exp \left[\left(\frac{-2}{b_o} \right) (x^2 + y^2) \right] \quad (4)$$

and

$$P = \frac{d^2 I_s}{d_o^2 (1 + v_o)} \exp \left(\left[\frac{-2}{b_o} \right] (x^2 + y^2) \right) \quad . \quad (5)$$

In the old probe volume model, it was sufficient that $I_{ac} > I_{min}$. The new intensity/visibility software filter, however, limits the intensity further by limiting the pedestal of acceptability.

To criterion that $I_{ac} > I_{min}$ is absolutely necessary but not sufficient, except for the first 4 bins which have no minimum pedestal intensity limitation.

The intensity/visibility software filter, which is contained in Table 1, was constructed such that P_{max} is proportional to d_{max}^2 . For instance for bin 35, $d_{max} = .595$ and $P_{max} = 271$. For bin 8, $d_{max} = .2185$.

$$\therefore P_{max_8} = \left(\frac{.2185}{.595}\right)^2 \times 271 = 36.5$$

Given that the visibility falls in any one bin, the actual pedestal scattered by the droplet has to fall between P_{min} and P_{max} , where P_{max} corresponds to the droplet moving through the center $x = y = z = 0$ of the probe volume. Given this visibility V there is a bin # associated which corresponds to a diameter d (as given by the visibility Table 2). The intensity/visibility software filter (included in Table 1) imposes the condition:

$$P = \frac{d^2 I_{s_1}}{d_o^2 (1+V_o)} \exp\left(\frac{-2y^2}{b_o^2}\right) > P_{min}$$

TABLE 1. VISIBILITY INTENSITY TABLE
(Called Table 3 by Software)

<u>BIN</u> <u>NO.</u>	<u>I_{MIN}</u> <u>(mV)</u>	<u>I_{MAX}</u> <u>(mV)</u>	<u>BIN</u> <u>NO.</u>	<u>I_{MIN}</u> <u>(mV)</u>	<u>I_{MIN}</u> <u>(mV)</u>
1	0	17	27	114	189
2	0	18	28	122	200
3	0	20	29	130	211
4	0	24	30	138	224
5	4	26	31	146	235
6	7	30	32	156	248
7	9	35	33	165	262
8	12	39	34	174	276
9	14	43	35	183	290
10	19	48	36	193	303
11	22	54	37	203	318
12	26	60	38	214	333
13	30	65	39	225	348
14	34	72	40	235	363
15	39	79	41	246	379
16	44	87	42	258	396
17	49	94	43	270	412
18	55	102	44	281	429
19	60	110	45	294	447
20	66	119	46	306	464
21	71	127	47	319	482
22	78	137	48	331	500
23	85	146	49	344	518
24	91	157	50	358	538
25	99	167	51	371	558
26	106	177	52	385	576
			53	399	597

TABLE 2. THE VISIBILITY FUNCTION

<u>BIN</u> <u>NO.</u>	<u>VIS</u> <u>LOW</u>	<u>VIS</u> <u>HI</u>	<u>REL</u> <u>BW</u>	<u>DIA/</u> <u>DELTA*CF</u>	<u>BIN</u> <u>NO.</u>	<u>VIS</u> <u>LOW</u>	<u>VIS</u> <u>HI</u>	<u>REL</u> <u>BW</u>	<u>DIA/</u> <u>DELTA*CF</u>
1	.986	.989	4	.0813	27	.645	.663	19	.4635
2	.981	.985	5	.096	28	.626	.644	19	.4782
3	.975	.98	6	.1107	29	.606	.625	20	.4929
4	.968	.974	7	.1254	30	.587	.605	19	.5076
5	.961	.967	7	.1401	31	.567	.586	20	.5223
6	.953	.96	8	.1548	32	.547	.566	20	.537
7	.944	.952	9	.1695	33	.527	.546	20	.5516
8	.935	.943	9	.1842	34	.506	.526	21	.5664
9	.924	.934	11	.1989	35	.486	.505	20	.5811
10	.914	.923	10	.2136	36	.466	.485	20	.5958
11	.902	.913	12	.2283	37	.446	.465	20	.6104
12	.89	.901	12	.243	38	.425	.445	21	.6252
13	.877	.889	13	.2577	39	.405	.424	20	.6399
14	.864	.876	13	.2724	40	.385	.404	20	.6546
15	.85	.863	14	.2871	41	.365	.384	20	.6692
16	.835	.849	15	.3018	42	.345	.364	20	.684
17	.82	.834	15	.3165	43	.326	.344	19	.6987
18	.804	.819	16	.3312	44	.306	.325	20	.7134
19	.788	.803	16	.3459	45	.287	.305	19	.728
20	.772	.787	16	.3606	46	.268	.286	19	.7428
21	.755	.771	17	.3753	47	.249	.267	19	.7575
22	.737	.754	18	.39	48	.231	.248	18	.7722
23	.72	.736	17	.4047	49	.213	.23	18	.7868
24	.701	.719	19	.4194	50	.195	.212	18	.8016
25	.683	.7	18	.4341	51	.177	.194	18	.8163
26	.664	.682	19	.4488	52	.16	.176	17	.831
					53	.143	.159	17	.8456

where P is measured by a peak detector of the Gaussian envelope and, therefore, it corresponds to $x=0$. I_{s1} and P_{\max} correspond to each other.

Given a bin #, there is a correspondence between diameter and pedestal,

$$\frac{P_{\min}}{P_{\max}} = 0.7 \frac{P(d_{\min})}{P(d_{\max})}$$

where:

$$P(d_{\min})/P_{\max} = \frac{d_{\min}^2 I_{s1}}{d_o^2 (1+V_o)} e^0,$$

$$\therefore P_{\min} = \frac{0.7 d_{\min}^2 I_{s1}}{d_o^2 (1+V_o)}.$$

Therefore,

$$I_{s1} = \frac{d_o^2 (1+V_o) P_{\min}}{0.7 d_{\min}^2} = \frac{d_o^2 (1+V_o) P_{\max}}{d_{\max}^2}.$$

Substituting for I_{s1} above:

$$P = \frac{d_{\max}^2 P_{\max}}{d_{\max}^2} \exp\left(\frac{-2y^2}{b_o^2}\right) > P_{\min}.$$

Solving for y

$$y = -\frac{b_o^2}{2} \ln \left(\frac{P_{min}}{K d^2} \right) , \quad (6)$$

where $K = \frac{P_{max}}{d_{max}^2}$ at any bin # .

For instance for bin #35, $K = \frac{.271}{.595^2} = .765$.

Note that the value of y will only remain constant if the characteristic size is d_{min} , in which case

$$\frac{P_{min}}{d_{min}^2} = 0.7 K ,$$

and $y = -\frac{b_o^2}{2} \ln 0.7 = .42 b_o^2$.

However, I have chosen $d_{character}$ to be the value given in the visibility table, which is larger than d_{min} ; therefore $y > 0.42$. For the high visibility bins, $d_{character} \gg d_{min}$; and, therefore, we should expect $y \gg .42$ as shown in the example. The expression for y based on the threshold and saturation intensity is given by:

$$y \leq -\frac{b_o^2}{2} \ln \left[\frac{I_{Th}}{I_s} \left(\frac{d_o}{d} \right)^2 \frac{(1+V_o)}{V} \right] - x^2 \quad (7)$$

Example

For the conditions:

$$I_{Th} = .0005V$$

$$I_s = .63V$$

$$d_o' = .845$$

$$V_o = .151$$

$$x \approx b_o$$

Also from Table 1 at bin # 35, $d' = .595$ and $P_{max} = .271V$ at $y = 0$.

$$I_{s1} = \frac{P d_o'^2 (1+V_o)}{d^2} = \frac{.271 (.845)^2 (1.151)}{.595^2} = .63V$$

$$K = \frac{.271}{.595^2} = .765$$

Therefore, Equation 6 yields: $y = -\frac{b_o^2}{2} \ln \left(\frac{P_{min}}{.765d^2} \right)$

where P_{min} is given in volts.

Equation 7 yields:

$$y < b_0 - \frac{1}{2} \ln \left[\frac{6.3 \times 10^{-4}}{d'^2 v} \right] - 1 \quad .$$

For example:

bin #	d'	v	P _{min}	$\frac{y(6)}{b_0}$	y(7)/b ₀
53	.8456	.15	.373	.436	1.25
35	.5811	.49	.171	.44	1.34
13	.2577	.88	.0278	.55	1.12
5	.1405	.965	.0042	.8	.84
4	.1254	.97	0	0	.77

Notice that the relationship between y and bin # would be a constant if for P_{min} I used the corresponding d_{min} instead of the d given on the V Table.

Upon obtaining y for each size class the size histograms are then unbiased by such values since they represent probability of collection.

4.0 THE IMAX TECHNIQUE

The method discussed here bases the size measurement on the absolute intensity scattered by the droplet crossing the probe volume, and the velocity measurement on the classical Doppler signal. It is referred to as the IMAX method. In situ single particle counters are limited because of the nonuniform profile (typically Gaussian) of laser beams. Under this condition a particle crossing the middle of the beam will scatter more light than a similar particle crossing through the edge. Therefore, the relationship between size and scattered light is not unique.

To circumvent this problem, two beams of unequal size are crossed such that the small beam identifies the middle of the large beam and therefore, remove the Gaussian ambiguity. Laser beams are chosen because of their spatial and temporal coherence and because of their size. These beams will interfere where they cross and a fringe pattern will be formed in the middle of the large beam. Signals exhibiting an ac modulation will have crossed the fringe pattern and therefore, the middle of the large beam. Both size and velocity of individual spherical particles can be extracted from this signal.

At least two approaches can be used to implement the above concept. The first consists of crossing two laser beams of different diameters but with the same wavelength. In the second two small beams of one wavelength cross in the middle of a larger beam of another wavelength. These approaches will now be explained starting with the second.

4.1 Two-Color System

Figure 4.1 illustrates the probe volume of this method. A spherical particle crossing through the fringes will also cross through a region of almost uniform intensity of the large beam. The ratio of the two beam diameters will establish the uniformity of the large beam intensity incident on the droplet.

If we refer to the small beam as 1 and the large beam as 2, the intensity profiles in the probe volume can be spectrally separated, and given by:

$$I_1 = 2I_{o1} \exp \left(-\frac{2}{b_{o1}^2} [x^2 + y^2 + z^2 \gamma^2 / 4] \right) \cdot \left[\cosh \left(\frac{2xy\gamma}{b_{o1}^2} \right) + \cos \frac{4\pi x \sin(\frac{\gamma}{2})}{\lambda} \right], \quad (8)$$

and

$$I_2 = I_{o2} \exp \left[-\frac{2}{b_{o2}^2} (x^2 + y^2) \right]. \quad (9)$$

Where I_o is the center intensity, γ is the intersection angle, b_o the waist radius, λ the laser wavelength, and x, y, z the coordinates. The z dependence of the large beam is negligible. If we also assume that $\frac{z\gamma}{2} \approx 0$ (which is an excellent assumption since a pinhole in the receiver

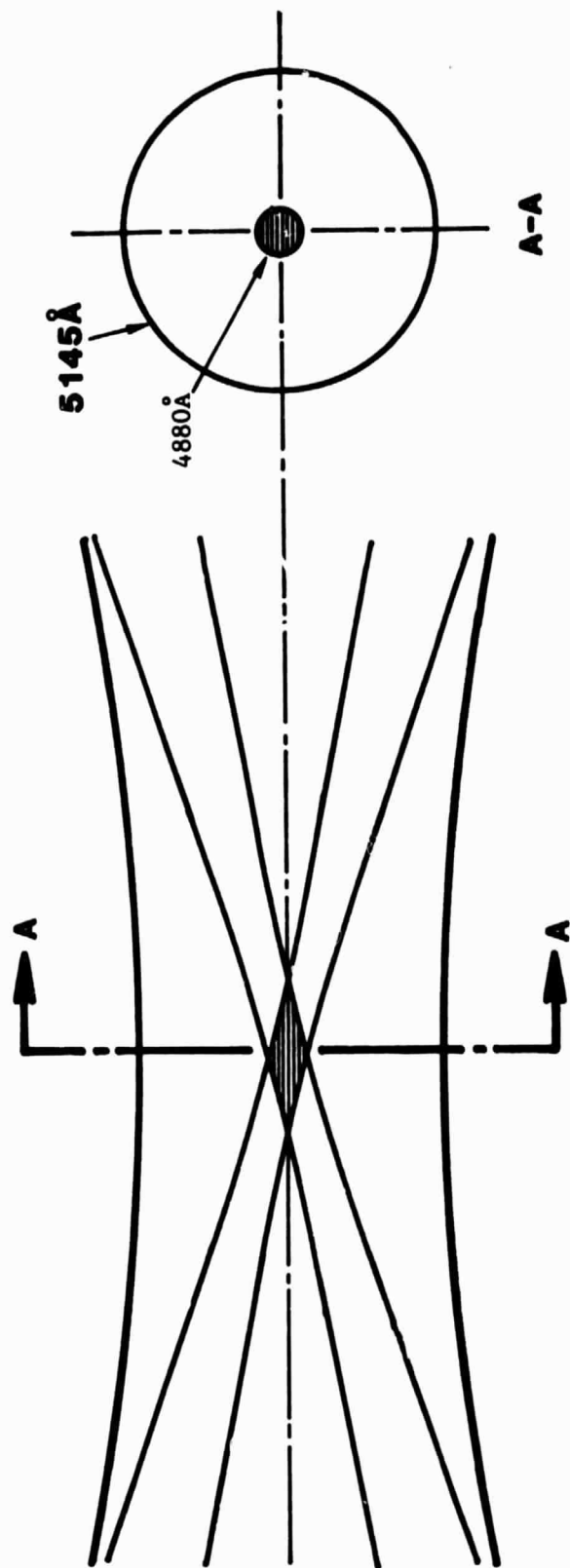


Figure 4.1.1. Probe Volume of Two Color IMAX Technique

will limit the value of z), the intensity scattered by a spherical particle is given by:

$$I_{s_1} = 2I_{o_1} K_{o_1} d^2 \exp \left[\left(-\frac{2}{b_{o_1}} \right) (x^2 + y^2) \right] \left[1 + \cos 2 \frac{\pi y x}{\lambda} \cdot V \right] , \quad (10)$$

and

$$I_{s_2} = I_{o_2} K_{o_2} d^2 \exp \left[\left(-\frac{2}{b_{o_2}} \right) (x^2 + y^2) \right] , \quad (11)$$

where

$$K_o = \frac{1}{4r^2} \int_{A_{\text{lens}}} \left[\epsilon^2(\theta, n) D(\theta) \right]_{\text{refraction}} + \left[\epsilon^2(\theta, n) D(\theta) \right]_{\text{reflection}} + \left[\frac{J_1^2(a \sin \theta)}{\sin^2 \theta} \right]_{\text{diff.}} dA . \quad (12)$$

K_o is a scattering coefficient, D is the divergence, n the index of refraction, ϵ the fraction of energy for every ray reflected or refracted, d is the diameter of a spherical particle, V is its

visibility, r the distance from the scattering center to the collecting lens, and θ the collection angle measured from the forward direction. It can be shown⁽¹⁵⁾ that the contributions of these three terms is a function of angle. To keep the following analysis simple we will choose a collection angle θ of 30° . Assuming that the solid angle of the collecting lens is small with respect to θ we can then compare the intensities scattered at the discrete angle $\theta = 30^\circ$.

The refraction or reflection terms are given by:

$$i_R = \alpha^2 \epsilon^2 D^2 ,$$

and the diffraction by:

$$i_D = \frac{\alpha^2}{\sin^2 \theta} J_1^2 (\alpha \sin \theta) .$$

where $\alpha = \frac{\pi d}{\lambda}$ is the size parameter, and J_1 the Bessel's function of the first kind. Reference 15 shows that for S polarization:

$$i(\text{refraction}) = 1.0375 \alpha^2$$

$$i(\text{reflection}) = 0.0785 \alpha^2$$

for $\xi = 30^\circ$ and it can be calculated that

$i_D(\alpha) < .088 \alpha^2$ for $\alpha > 49$ ($d > 7.6 \mu\text{m}$). At this angle the combined reflected and diffracted light represent 16% of the refracted light.

Which implies that, in general, the three components must be taken into account. It is assumed that the collecting lens is in the plane of symmetry of the crossing beams. The above equations show that the scattered light intensity is proportional to the square of the diameter of the sphere. This approximation is only valid for diameters larger than about 10 wavelengths. Note that the angle θ (deviation of incident pencil of light) to an arbitrary position of the lens is different for both beams (except on the line of symmetry). However, the integrated value is the same as long as the collecting lens is in the plane of symmetry. In this technique the ac modulation of I_{s1} is used to establish detectability of the signal and to measure the velocity. For a given threshold level, the larger the dynamic size range, the farther from the center of the beam the largest particle can cross and still exhibit ac modulation and, therefore, be detectable. This will introduce an error in the measurement as will be discussed in the next section.

The peak to peak ac signal is then given by:

$$I_{ac1} = 4 I_{o1} K_{o1} v d^2 \exp \left[\left(- \frac{2}{b_{o1}^2} \right) (x^2 + y^2) \right] \quad , \quad (13)$$

and the pedestal is given by:

$$P_1 = 2 I_{o1} K_{o1} d^2 \exp \left[\left(- \frac{2}{b_{o1}^2} \right) (x^2 + y^2) \right] \quad . \quad (14)$$

Dynamic size range and error analysis

There are two known sources of error in the IMAX method. First is the error introduced by beam blockage produced by other particles in the trajectory of the beams and scattered light. This one is difficult to quantify and will be discussed with the results. Second, since the small beam has a finite diameter the particles can travel a small distance away from the center of the big beam and still cross sufficient fringes to be detectable. The farther from the center it can be detectable, the larger the error it can produce. It will be shown here that this error increases with dynamic size range, and decreases with ratio of the large to small beam.

The dynamic range is limited by the electronic and optical noise. In general, we can establish that there is a threshold to the minimum processible ac signal, and a saturation level associated with the largest signal processible by the electronics. All the processible signals must fall between these two limits. Equation 13 gives the peak to peak ac signal. Notice that both the diameter (d) and the visibility (V) influence the above expression.

To simplify this analysis we will neglect the contribution of diffraction, that is the collection angle will be off-axis. Single particle counters usually collect off-axis light ($\theta > 30^\circ$) for the sake of producing a small probe volume. Therefore, the above assumption is very reasonable for spheres larger than $7 \mu\text{m}$. The dynamic range is actually larger when diffraction is included.

The minimum processible ac signal is produced by the smallest particle (with diameter d_{\min}) crossing the probe volume at $y = 0$ and crossing the minimum number of fringes required by the electronics ($x = b_{o1}$).

Therefore, $I_{ac_{\min}} = 4I_{o1} K_{o1} d_{\min}^2 \exp(-2)$ where it has been assumed that the visibility of the smallest particle is 1.

The maximum ac signal is produced by a droplet of diameter d_o (not necessarily d_{\max}) and visibility V_o .

$$I_{ac_{\max}} = 4I_{o1} K_{o1} d_o^2 V_o \exp \left[\left(-\frac{2}{b_{o1}^2} \right) (x^2 + y^2) \right] \quad (15)$$

The farthest from the center this particle can be detected is when:

$$I_{ac_{\max}} = I_{ac_{\min}}$$

and it crosses sufficient number of fringe ($x = b_{o1}$). Therefore,

$$4I_{o1} K_{o1} d_o^2 \exp \left[\left(-\frac{2}{b_{o1}^2} \right) (b_{o1}^2 + y^2) \right] = 4I_{o1} K_{o1} d_{\min}^2 \exp(-2) \quad .$$

Solving for the size range, we obtain:

$$\left(\frac{d_o}{d_{\min}}\right) = \frac{\exp(-2)}{V_o} \exp\left[\frac{2(b_{o1}^2 + y^2)}{b_{o1}^2}\right] = \frac{1}{V_o} \exp\left(\frac{2y^2}{b_{o1}^2}\right),$$

and

$$2y^2 = b_{o1}^2 \ln\left[\left(\frac{d_o}{d_{\min}}\right)^2 \frac{V_o}{\exp(-2)}\right] - 2b_{o1}^2,$$

which results in

$$2y^2 = b_{o1}^2 \ln\left[V_o\left(\frac{d_o}{d_{\min}}\right)^2\right]. \quad (16)$$

The error in the size will be due to an error in the intensity scattered by the large beam when the particle crosses at $y > 0$ (notice that the particle must cross through $x = 0$). If we state that the large beam is m times larger than the small one,

$$\frac{I_{s2}}{I_{o2} K_{o2} d^2} = \exp\left(\frac{-2y^2}{m b_{o1}^2}\right). \quad (17)$$

To simplify the error analysis, let us assume that the optical parameters are chosen such that for any size range the visibility of the largest droplet is larger than zero.

That is $V(d_{\max}) > 0$ and $d'_{\max} < 1$ where $d'_{\max} = 1$ produces the first zero in the visibility. Then the maximum ac signal is produced by a particle of diameter $d_0 = 0.626 d_{\max}$ and its visibility is 43%.

Substituting these values into Equation 16, we obtain:

$$\frac{2y^2}{b_{o1}^2} = \ln \left[.1685 \left(\frac{d_{\max}}{d_{\min}} \right)^2 \right] .$$

The maximum errors resulting from the finite size of the beams can now be presented in tabular form (m is the ratio of large to small beams at the probe volume).

m	d_{\max}/d_{\min}	$\frac{2y^2}{b_{o1}^2}$	$\frac{I_{s2}}{I_{o2} K_{o2}^2}$	max error
7	10	2.82	.94	3%
7	20	4.21	.92	4%
7	30	5.02	.90	5%
5	10	2.82	.89	5%
5	20	4.21	.85	8%
5	30	5.02	.82	10%

4.2 Single Color System

Figure 4.2 shows a schematic representation of the probe volume formed by crossing two beams of the same wavelength but different diameters. There are several fundamental differences between this and the two color system: 1) Fringes are formed everywhere the large and small beams mix; 2) The pedestal of the large beams can not be spectrally separated but electronically filtered. The intensity distribution of either beam can be expressed as:

$$I_1 = I_{o1} \exp \left[-\frac{2}{b_{o1}^2} (x^2 + y^2) \right] , \quad (18)$$

and

$$I_2 = I_{o2} \exp \left[-\frac{2}{b_{o2}^2} (x^2 + y^2) \right] . \quad (19)$$

The intensity scattered by the spherical particle can be expressed by:

$$I_s = I_{s1} + I_{s2} + 2 I_{s1} I_{s2} \cos \beta \cdot V$$

where

$$I_s = I K_o d^2 .$$

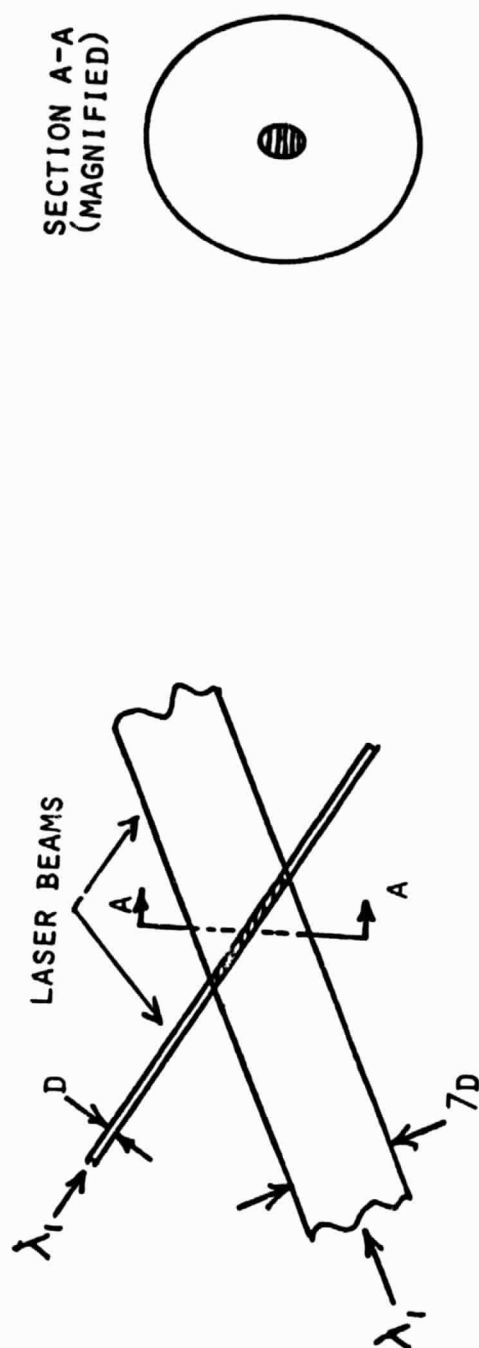


Figure 4.3.3. Probe Volume of Single Color IMAX Technique

β is the phase angle, and again it is assumed that the collecting lens is on the plane of symmetry of the two crossing beams. The pedestal is given by

$$P = I_{s_1} + I_{s_2}$$

and the peak to peak ac intensity:

$$I_{ac} = 2 I_{s_1} I_{s_2} V (\cos \beta = 1) - 2 I_{s_1} I_{s_2} V (\cos \beta = -1)$$

$$= 4 I_{s_1} I_{s_2} V .$$

That is,

$$P = I_{o_1} K_o d^2 \exp \left[-\frac{2}{b_{o_1}^2} (x^2 + y^2) \right] + I_{o_2} K_o d^2 \exp \left[-\frac{2}{b_{o_2}^2} (x^2 + y^2) \right] , \quad (20)$$

and

$$I_{ac} = 4K_o I_{o_1} I_{o_2} d^2 V \exp \left[-\frac{(x^2 + y^2)}{b_{o_1}^2} - \frac{(x^2 + y^2)}{b_{o_2}^2} \right] . \quad (21)$$

Following the same approach as before, and again neglecting the contribution of diffraction for the off-axis collection angle. If we let

$m = b_{o2}/b_{o1}$, we obtain:

$$I_{ac_{min}} = 4K_o I_{o1} I_{o2} d_{min}^2 \exp \left[-1 - \frac{1}{m} \right] \quad , \quad (22)$$

$$I_{ac_{max}} = 4K_o I_{o1} I_{o2} d_o^2 V_o \exp \left[-\frac{(b_{o1}^2 + y^2)}{b_{o1}^2} - \frac{(b_{o1}^2 + y^2)}{m^2 b_{o1}^2} \right] \quad . \quad (23)$$

The variation in y will result in an error of the measured pedestal. If we can assume that m is large, then the pedestal of the large beam can be recovered by electronic filtering and it is given by the second term of Equation 20. This variation in y is obtained equating 22 and 23, and we obtain

$$y^2 = \frac{m^2 b_{o1}^2}{m^2 + 1} \ln \left[\frac{d_o^2 V_o}{d_{min}^2} \right] \quad . \quad (24)$$

The error in the size will result from droplets crossing the pedestal of the large beam at $x = 0$ and y given by 24. That is:

$$-\frac{I_{s2}}{I_{o2} K_o d^2} = \left[\frac{-2y^2}{m^2 b_{o1}^2} \right] \quad . \quad (25)$$

Making similar assumptions as before:

$$d_o = .626 d_{\max} \text{ and } V_o = 0.43$$

$$\therefore \frac{2y^2}{m^2 b_{o1}^2} = \frac{2}{m^2 + 1} \ln \left[.1685 \left(\frac{d_{\max}}{d_{\min}} \right)^2 \right] \quad (26)$$

The maximum errors resulting from the finite size of the beams can be presented in tabular form (m is the ratio of large to small beams in the probe volume):

m	d_{\max}/d_{\min}	$\frac{2y^2}{m^2 b_{o1}^2}$	$\frac{I_{s2}}{I_{o2} K_{o2} d^2}$	max error
7	10	.113	.89	5%
7	20	.168	.84	8%
7	30	.2	.82	10%
5	10	.22	.80	10%
5	20	.32	.72	15%
5	30	.39	.68	18%

It should be pointed out that the technique discussed here bases the detectability of the signal on the modulated or ac part of the scattered light. It is, therefore, important that no zeros are present in the visibility function.

4.3 A Self-Calibrating Algorithm Combining IMAX with V/I

SPC's based on absolute scattered light require calibration at one datum point. When measuring dense sprays, beam attenuation will make this calibration difficult. An algorithm is discussed here that will eliminate this problem.

The algorithm is based on measuring the visibility of any size class droplet. Combining the visibility and intensity⁽¹⁶⁾ of the signal a very accurate measurement of such size can be made. Knowing the size of the chosen corresponding visibility one can then establish the amplitude of the pedestal of this signal by adjusting the gain to the photodetector. The logic is as follows: for a given visibility (chosen in the most accurate region of the visibility function) there is an associated size and, therefore, an intensity scattered from the large beam. Since the intensity of this large beam is almost uniform the scattered light associated with the chosen visibility will be almost constant in the absence of errors in the visibility. There are, however, errors associated with measuring visibility in a dense spray and these points are rejected by $V/I^{(16)}$. The process is an iterative one where V/I is implemented by choosing several narrow intensity bands to establish points out of control. The gain to the photodetector is adjusted until the majority of the points fall in the pre-established intensity band corresponding to the measured size.

4.4 The IMAx Probe Volume

The dynamic range exercise indicated that droplets that scatter light with large modulation are detectable over a larger region than those that scatter light with little modulation. As a result, the probe volume or region of detectability is a function of droplet size. Algorithms have been presented⁽¹⁷⁾ to define the probe volume in LDV type systems. A very simple algorithm will be presented here for the two color system and off-axis collection.

Notice that only the small beams define the probe volume in this case and, therefore, the probe volume will be a standard LDV type volume. The approach followed will be very similar to the one described in Reference (17).

There are two signal levels imposed by the electronics: the saturation (I_{\max}) and the threshold (I_{\min}). The intensity to the peak of the ac modulation (I_{peak}) of the largest signal must be less than I_{\max} , and the smallest detectable signal must be larger than I_{\min} (defined peak to peak).

$$I_{\text{peak}_1} = 2I_{o_1} K_{o_1} d_o^2 (1+V_o) < I_{\max} \quad . \quad (27)$$

where d_o produces the largest signal within the detectable size range, and V_o is its corresponding visibility.

Solving for I_{o_1} we obtain:

$$I_{o_1} = \frac{I_{\max}}{2K_{o_1} d_o^2 (1+V_o)} \quad . \quad (28)$$

This expression can now be substituted in Equation 13 to obtain:

$$I_{ac_1} = \frac{2d^2 V I_{\max}}{d_o^2 (1+V_o)} \exp \left[\left(-\frac{2}{b_{o_1}^2} \right) (x^2 + y^2) \right] , \quad (29)$$

and the detectability criterion establishes that $I_{ac_1} > I_{\min}$ and that sufficient fringes are crossed. If we assume that the number of fringes processed by the electronics is equal to that in the waist diameter, $x = b_{o_1}$.

Solving for y in Equation 29 we obtain:

$$y < -\frac{b_{o_1}^2}{2} \ln \left[\frac{I_{\min}}{2I_{\max}} \left(\frac{d_o}{d} \right)^2 \frac{(1+V_o)}{V} \right] - b_{o_1}^2 . \quad (30)$$

The cross-sectional area of sensitivity for an off-axis pinhole limited signal can be approximated by:

$$A(d) = \frac{2D_p y}{\sin \theta} \cdot \frac{f_1}{f_2} , \quad (31)$$

where D_p is the pinhole diameter and f_1/f_2 determines the magnification of the receiving optics. The effect of the pinhole and the coordinate system are illustrated on Figure 4.3.

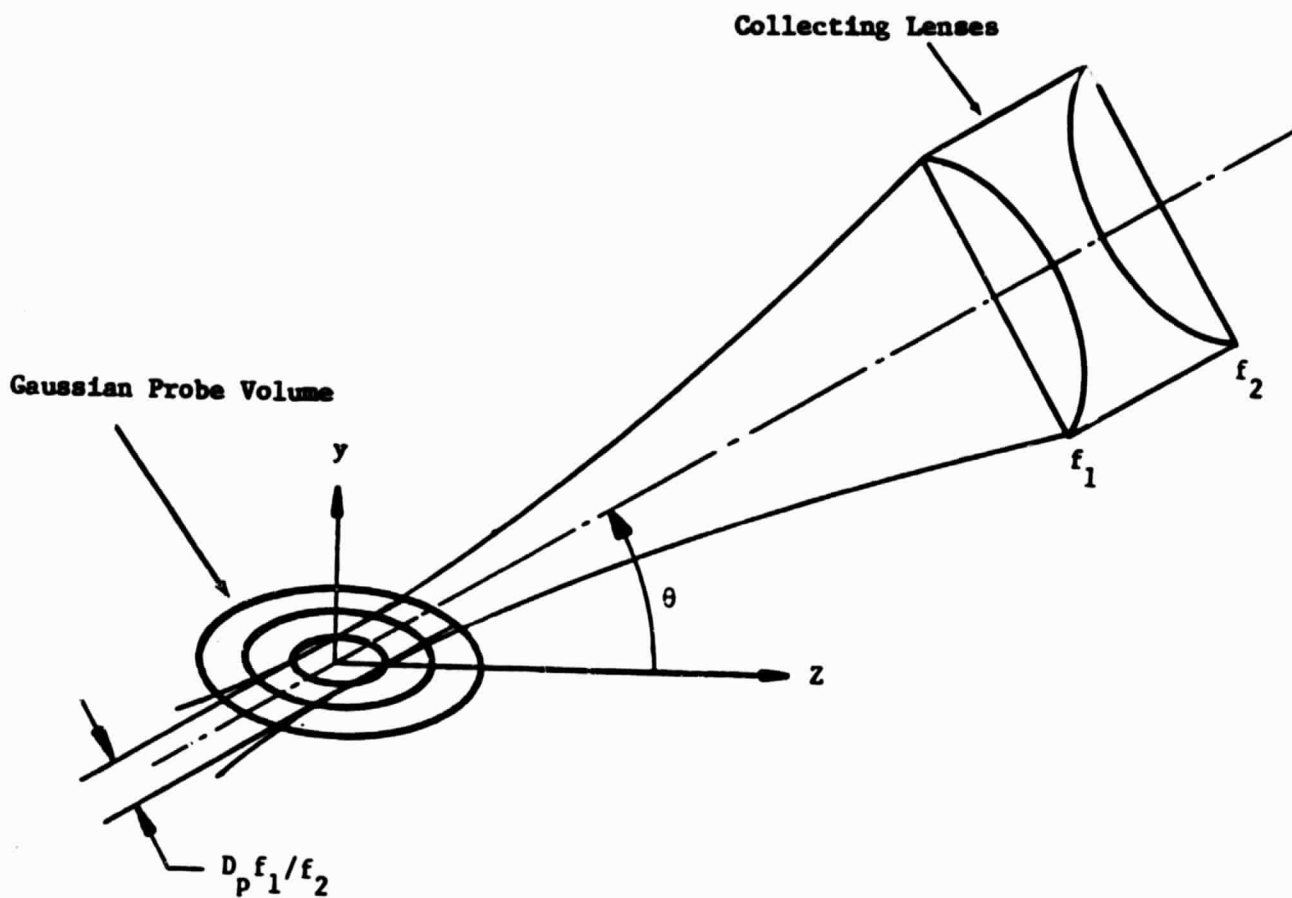


Figure 4.3. Schematic Representation of Dual Beam Probe Volume Limited by a Pinhole

As seen by Equation 30 and 31 the area of detectability (in the y,z plane) is only a function of droplet size and corresponding visibility. This area can now be normalized and provide a weighting function to size distributions otherwise biased to the large signals.

This weighting factor is given by:

$$w(d) = \frac{A(d)}{A_{\max}} \quad .$$

The number density of any size droplet can also be calculated by dividing the number of counts of the given size by its corresponding sampling volume (SV).

The sampling volume is a cylinder with cross-section $A(d)$ and length equal to the droplet velocity ($U(d)$) multiplied by the effective sampling time (T).

That is $SV(d) = A(d)U(d)T$, and $T = TS - \sum_{i=1}^M N \tau_{D_i} - M\tau_0$, where TS is the total sampling time to collect M samples, N is the number of fringes, τ_{D_i} is the Doppler period of sample i and τ_0 is the processor's dead time after every sample.

The number density of size d is then given by:

$$ND(d) = \frac{N(d)}{A_{\max} U(d)T} \quad , \quad (32)$$

where $n(d)$ is the raw count of size d . Because of the multivalued characteristic of the visibility curve, V_0 should be larger than the first zero of the visibility function. Equation (10) defines the abscissa of this function as $d' = \frac{d}{\delta CF}$. This value should be kept smaller than one, however, physical constraints render this not always possible. The collection factor (CF) can be easily changed almost linearly by changing the collection F#. In the experiments reported here this was done by placing a mask on the path of light scattered by the small beams. As an example, the spray data shown on Figures 4.9A and 4.9B correspond to $I_{\min} = .6 \times 10^{-3}$ V, $I_{\max} = .7$ V (these intensities are read directly in volts). Since very little data was measured above 160 μm , the mask was chosen to obtain $d' = 1$ at about 160 μm . Therefore

$$d'_0 = \frac{200}{\delta CF} = \frac{200}{160} = 1.24.$$

The following values are then obtained for the nondimensional diameter (d'), its visibility (V) and the normal probe volume dimension (y , as given by Equation 30).

d	20	40	60	80	100	120	140	160	180	200
d'	.12	.25	.37	.5	.62	.75	.87	1.0	1.12	1.24
V	.97	.88	.76	.6	.43	.27	.12	.02	.08	.12
y	.35	.9	1.06	1.14	1.17	1.15	1.03	.55	1.05	1.19

Similar calculations were performed for the size ranges 5 to 50 μm , and 10 to 100 μm .

4.5 Description of IMAX Breadboard

Figure 4.4 shows a schematic diagram of the two-color breadboard system. An argon-ion laser provides the light source. The beam colors are separated by the dispersion prism and two of these colors (the 5145Å shown by the broken line, and the 4880Å shown by the solid line) are used to define the probe volume. A beam expander formed by lenses L1 and L2 define the beam ratio parameter m . A compensated beamsplitter splits the blue beam into two beams and the transmitting lens L3 focuses and crosses these two blue beams in the middle of the green beam. The receiving optics use a dichroic mirror to separate the two colors of the scattered light. The probe volume is imaged on pinholes in front of two PMT's and interference filters are used to perfectly separate the two colors. The outputs of the two PMT's are then electronically processed as shown on Figure 4.5, and information of the size and velocity of individual spheres crossing the probe volume is thus obtained. An electronic processor was developed for this purpose, and a dedicated micro-processor was interfaced to store, display and analyze the acquired data. Sample rates of several KHz are possible with this system.

4.6 Results Obtained with the IMAX Technique

Experimental results are presented to illustrate the accuracy and resolution of the IMAX technique.

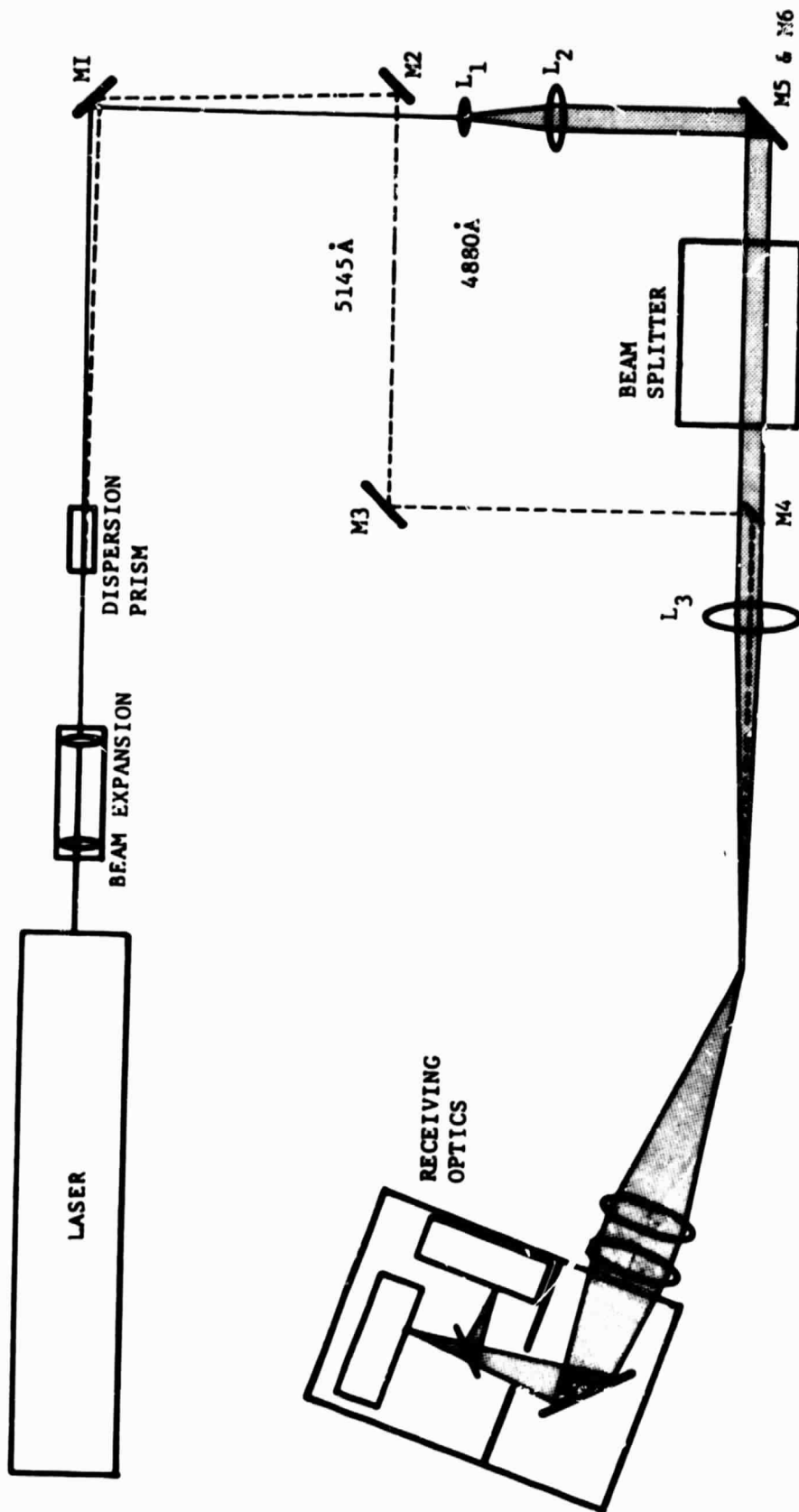


Figure 4.4. Schematic IMAX Breadboard System

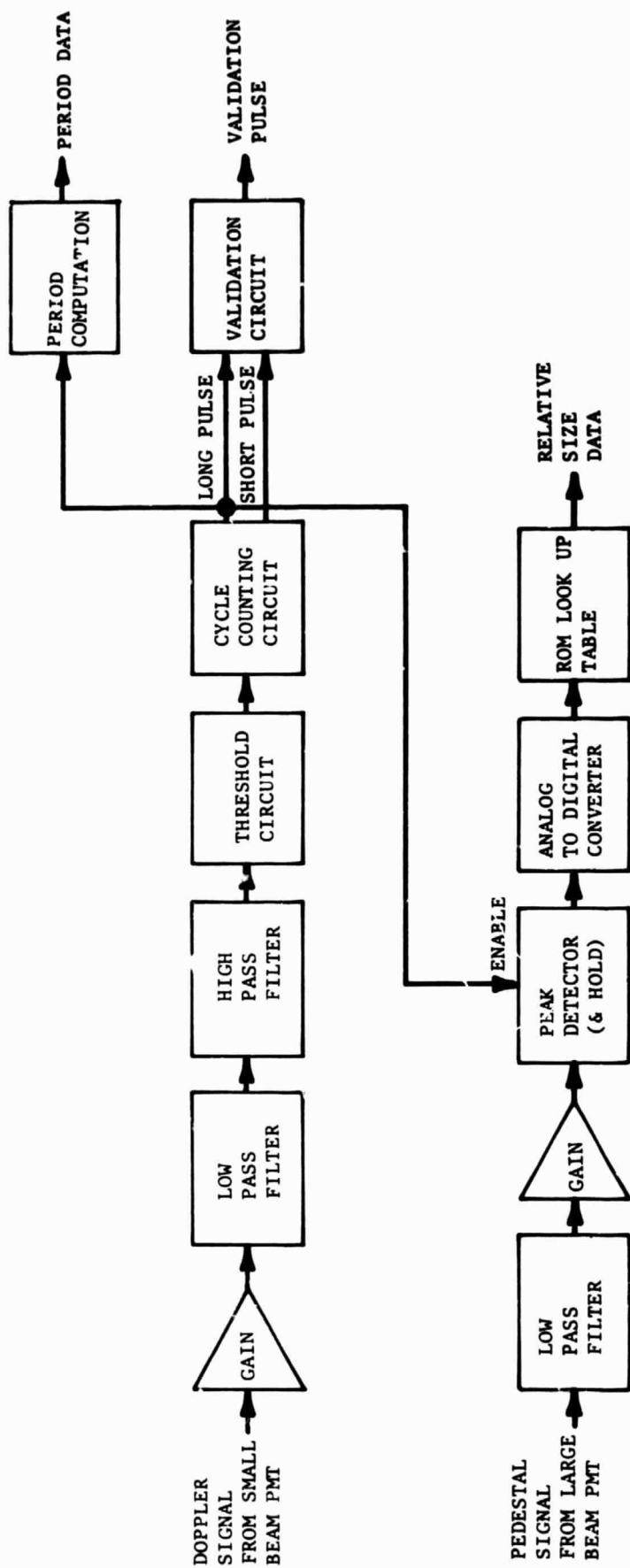


Figure 4.5. Electronics Block Diagram
Droplet Sizing, Two Color IMAX Technique

IMAX Measurements with the Berglund Liu Droplet Generator

A vibrating orifice droplet generator was used to produce strings and sprays of known size droplets. The procedure used in these experiments was to produce a string of large monodispersed droplets to calibrate the instrument. Smaller droplets were then produced by increasing the frequency of vibration of the orifice, and with the dispersion air a spray of these droplets was formed. The spray angle was about 10° and the number density was typically $500/\text{cm}^3$. The optical configuration consisted of a transmitting lens of 711 mm, $m = 7$, blue waist diameter of 100 μm , receiving angle of 20° , and receiving lenses of 300/495 mm. The calibration point was provided by a string of 110 μm droplets produced with a flow rate of $0.21 \text{ cm}^3/\text{min}$ and a frequency of 5 KHz.

Figure 4.6 shows the measured size and velocity. A spray of primary droplets of 49 μm (produced with a flow rate of $0.21 \text{ cm}^3/\text{min}$ and frequency of 56.9 KHz) was then produced with the dispersion air.

Figure 4.7a shows the measurements of the spray of primary droplets.

Figure 4.7b shows the measurements of a spray formed of primary droplets and doublets. The theoretically predicted sizes are 49 μm and 62 μm .

The sizes actually measured were 46 μm and 57 μm respectively.

Figure 4.7c extends the measurements of 4.7b to the presence of triplets. The theoretically predicted sizes in this case are 49 μm , 62 μm and 70 μm . Note that the measured diameters of the doublets and triplets are related to the primary droplets by $2^{1/3}$ and $3^{1/3}$ respectively.

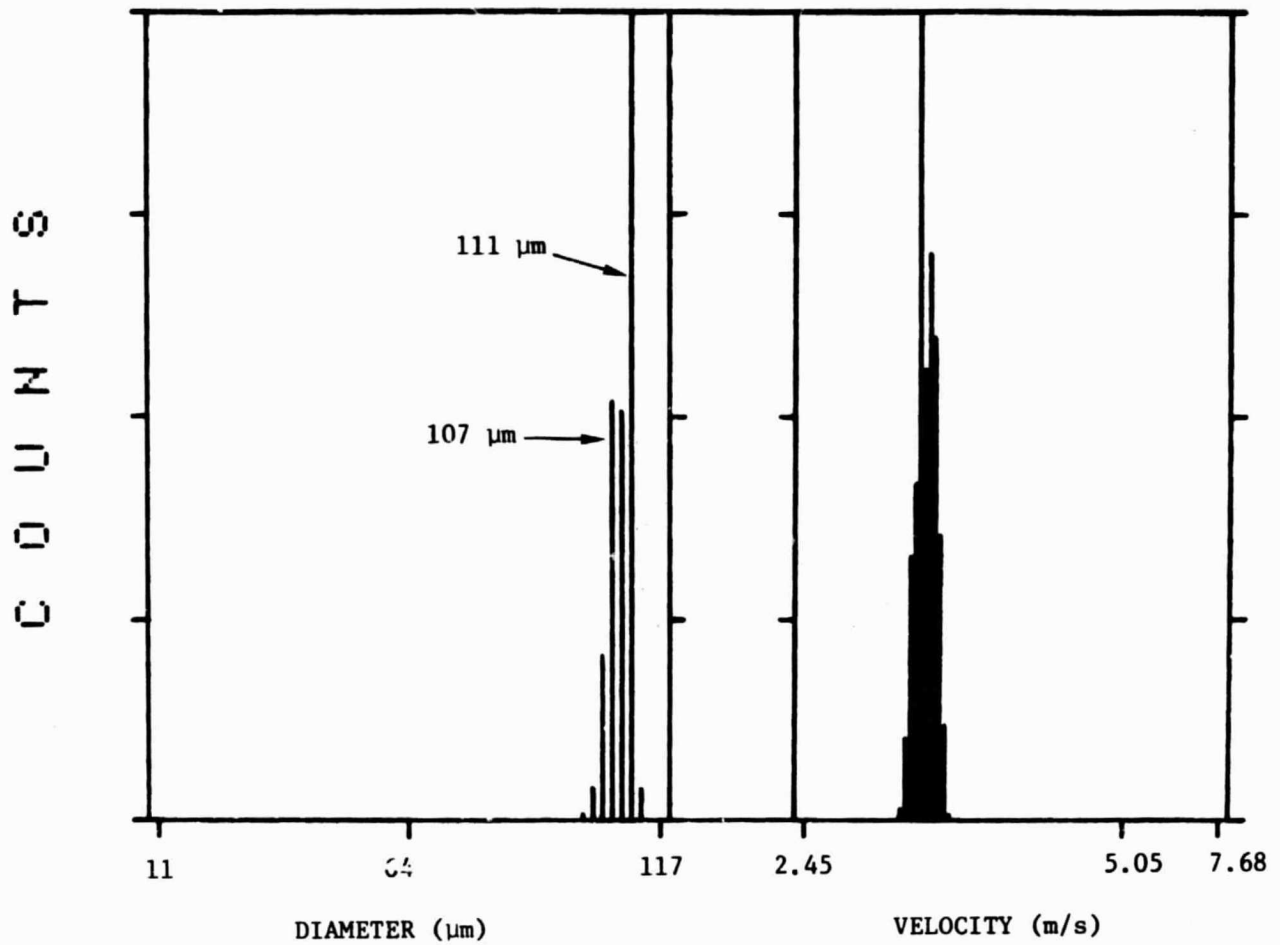


Figure 4.6. IMAX Measurements on String of Monodispersed Droplets

IMAX DROPLET SIZE MEASUREMENTS

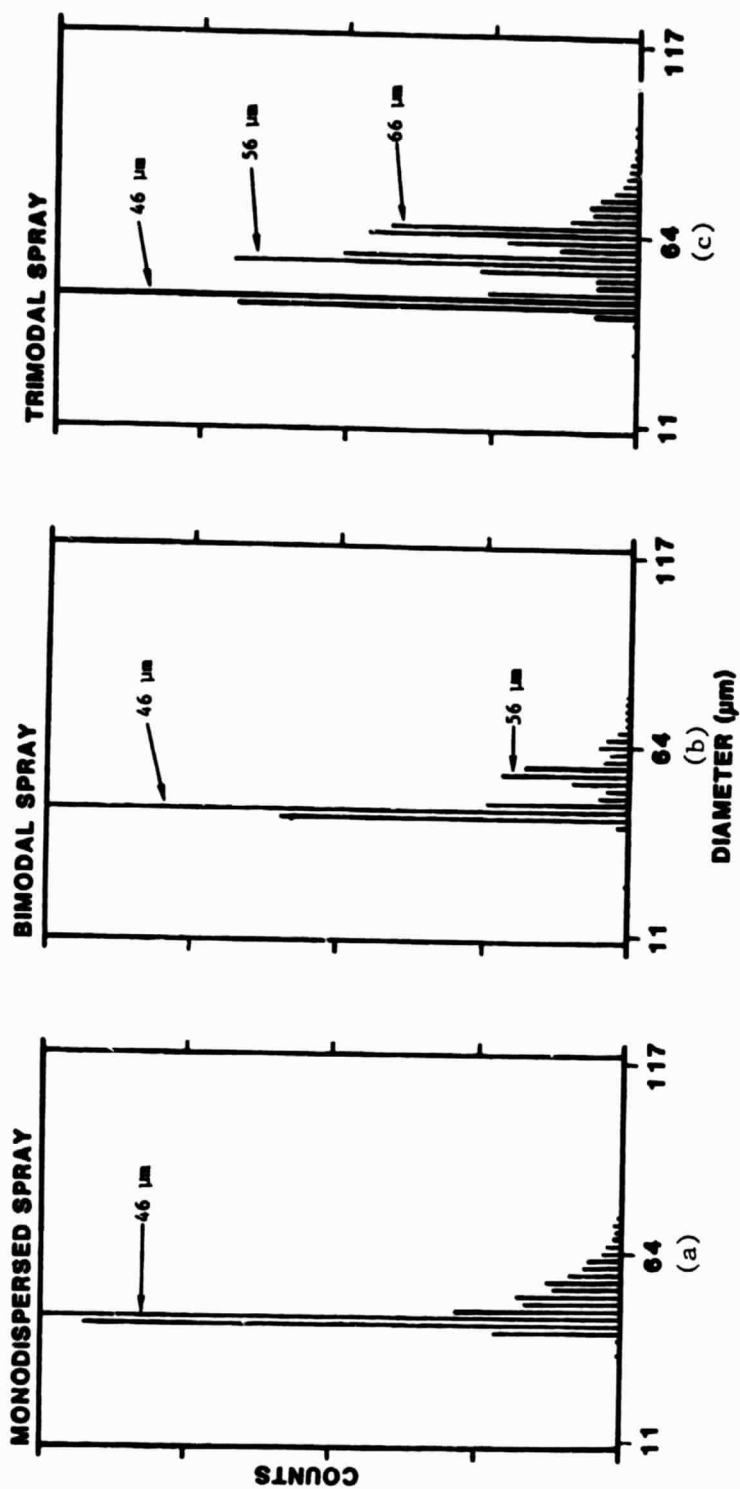


Figure 4. /

Effect of beam blockage on size distribution

The effect of spray blocking the laser beams before they cross on the size distribution measured with IMAX was explored. A size range of 10 to 100 μm was used in this case, and the monodispersed droplet size was 73 μm .

Figure 4.8a shows the measurement of the monodispersed string of droplets.

Figure 4.8b shows similar results but a spray is blocking the laser beams. Two effects can be noted: the peak of the distribution dropped to 69 μm (5%) and the spread of the distribution is +5 μm , -7 μm (+7%, -10%), to the $1/e^2$. It should be noted that once the high voltage is corrected to account for the beam blockage, the broadening should have very little effect in the distribution of a polydispersed spray.

Spray measurements with IMAX

Measurements of a spray produced by a pressure nozzle (Spraying Systems TGO.3 at 50 psi) were conducted with IMAX. They were made at 30 mm from the nozzle tip and at two radii: 0 and 10 mm. The results are shown on Figures 4.9a and 4.9b. The trend shown by the two plots is the expected one. That is, there are more small droplets in the middle of the spray than on the edge.

In order to test the resolution of the system, data were obtained using three different size ranges: 5 to 50 μm ; 10 to 100 μm ; and 20 to 200 μm . This is one of the most difficult self-consistency tests imposed on any technique, and most available techniques will show a shift on the predicted data. IMAX shows excellent matching of the data in the overlapping region as illustrated in Figures 4.9a and 4.9b.

EFFECT OF BEAM BLOCKAGE ON SIZE DISTRIBUTION

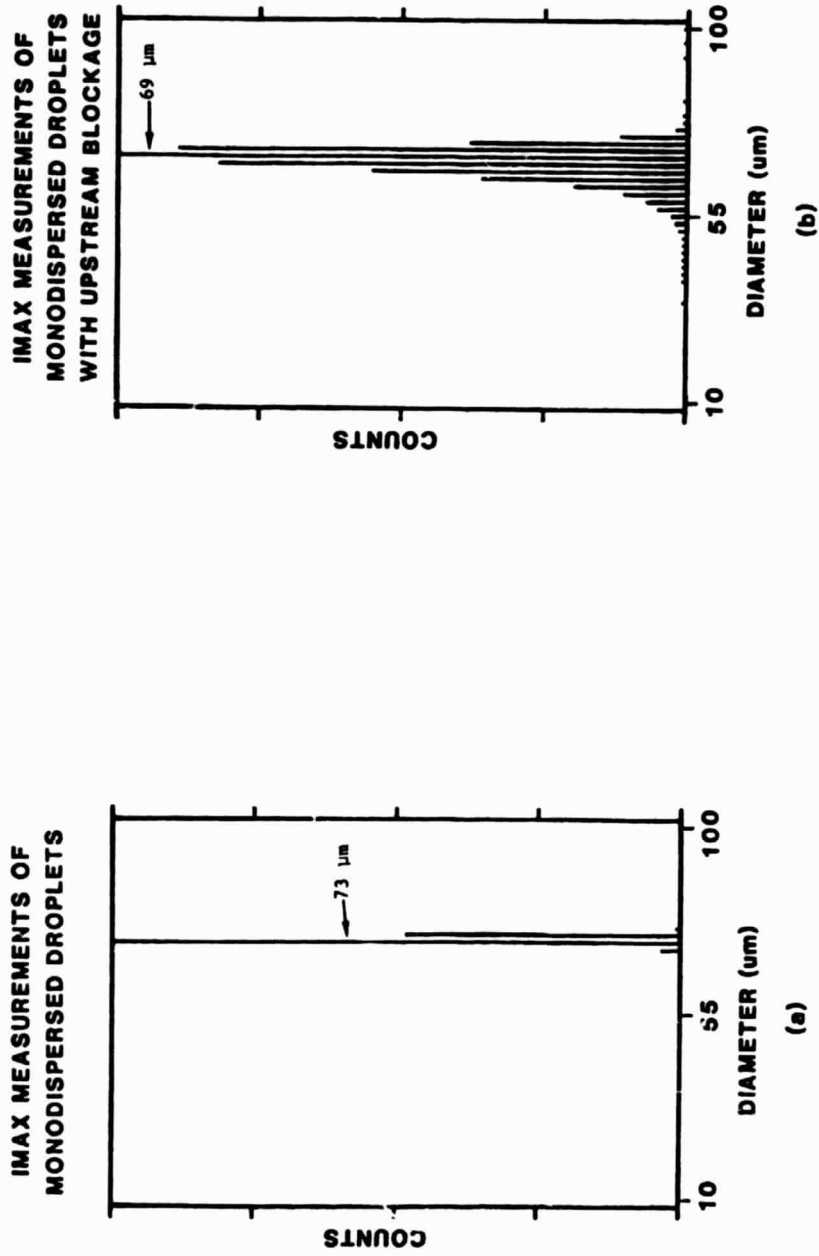


Figure 4.8

SPRAY CHARACTERIZATION WITH IMAX

NOZZLE: SPRAYING SYSTEMS FULL CONE TGO.3

PRESSURE: 50 psig

POSITION: AXIAL = 30 mm RADIAL = 0

<u>SYMBOL</u>	<u>SIZE RANGE</u>	<u>SERIES</u>
□	20 - 200 μ m	SNM/30
△	10 - 100 μ m	SNM/10
○	5 - 50 μ m	SNM/50

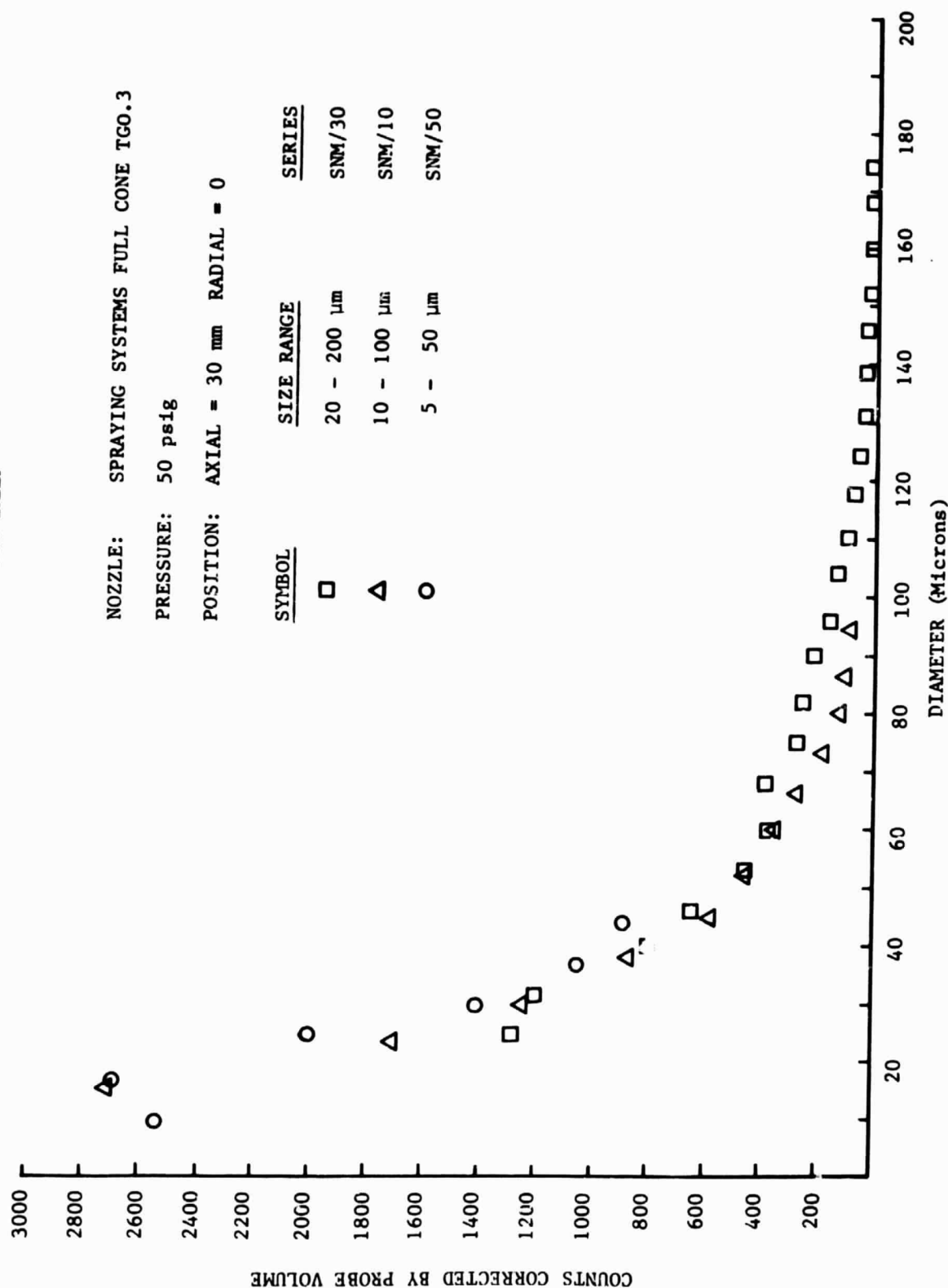


Figure 4.9a. Size Distribution in the Center of a Full Cone Spray

SPRAY CHARACTERIZATION WITH IMAX

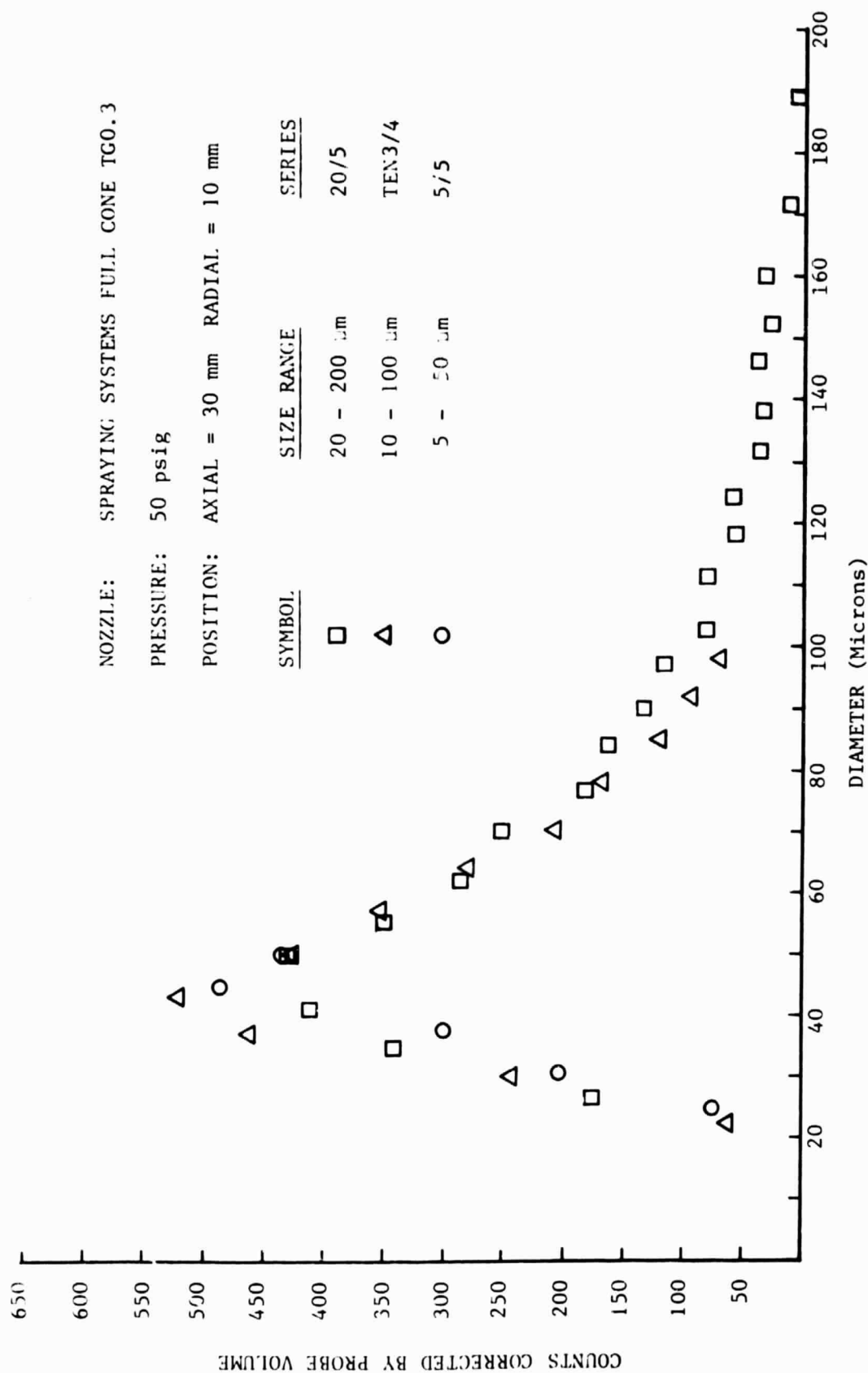


Figure 4.9b

The corresponding droplet velocity distributions are shown on Figures 4.10a and 4.10b. It can be observed that the droplets are moving faster at the edge of the spray than in the center. This results from the large momentum and terminal velocity associated with the large droplets present at the edge of the spray.

NOZZLE: SPRAYING SYSTEMS FULL CONE TGO.3

PRESSURE: 50 psig

AXIAL POSITION: 30 mm

RADIAL POSITION: 0

RADIAL POSITION: 10 mm

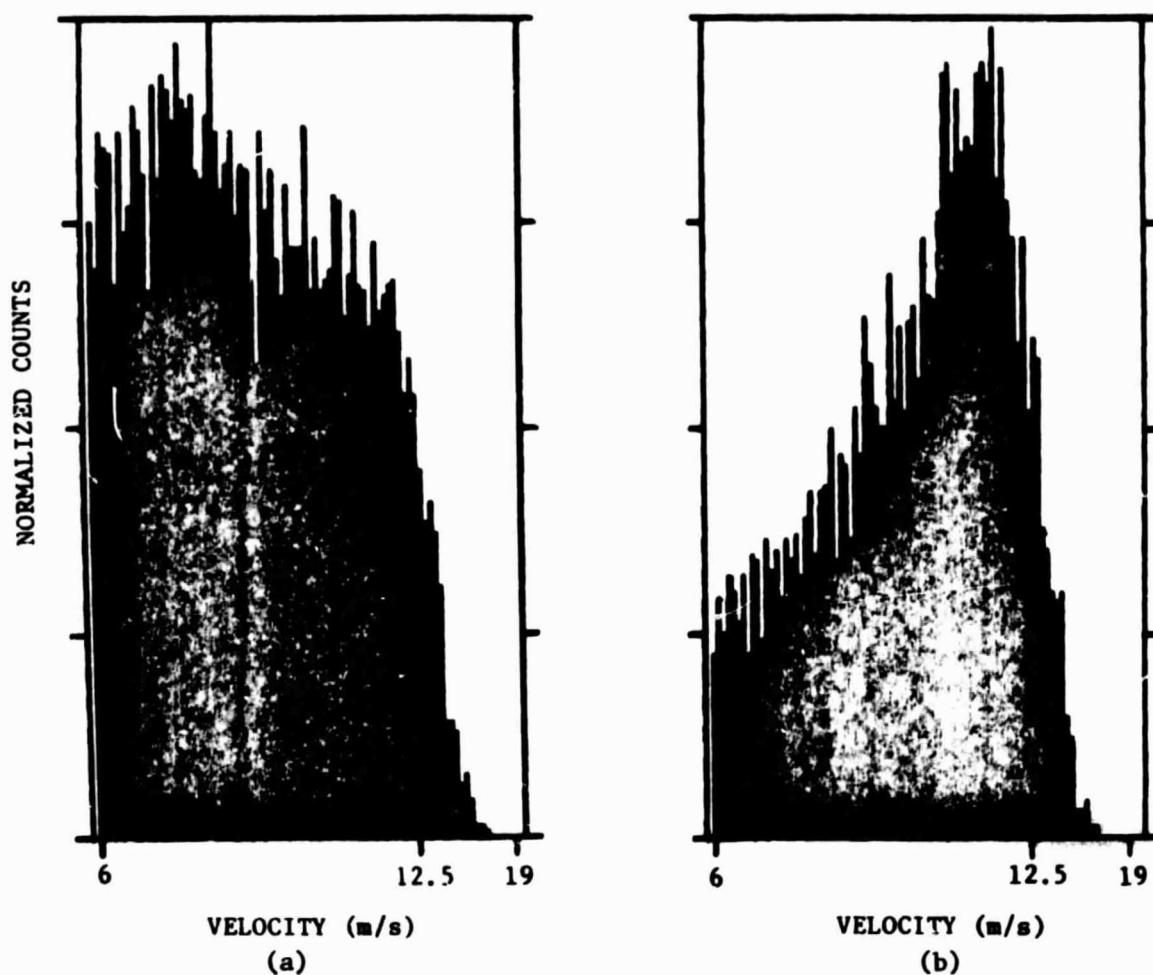


Figure 4.10. Velocity Distributions at Two Radial Positions of a Full Cone Spray

5.0 THE ADVANCED DROPLET SIZING SYSTEM (ADSS)

An instrument was developed using the concepts described before. This instrument is a sophisticated optical and electronic system for the measurement of various parameters of liquid droplets moving in a gaseous medium. It may be configured to employ either of two different techniques to measure size distributions of individual droplets.

These are:

Visibility-Intensity	V-I
Absolute Intensity	IMAX

In either configuration measurement of velocity is by the conventional laser Doppler technique. The instrument is capable of displaying a variety of different raw or reduced data sets as either histograms or correlations between velocity and size.

Accuracy depends on careful attention to the details dealing with alignment and operating procedures as outlined in the ADSS operating manual (18).

The hardware system comprizes the following separate pieces of equipment for the SDL V-I / IMAX ADSS:

Transmitter

Receiver

V-I / IMAX Interface Box

VP 1001 Visibility Processor (6FP)

Data Management System (6FP)

Keyboard (6FP)

Krohn-Hite Filter

Miscellaneous Cables

Software Media

Operating Manual

The accompanying software is supplied on 5 1/4 inch floppy disc media for operation on the DMS.

A photograph of the optical transmitter and receiver is shown in Figure 5.0. The electronic components are shown on Figure 5.1.

A schematic representation of the interconnections within the entire ADSS is shown in Figure 5.2.

This section describes the transmitter, receiver, and V/I interface box. The electronic processor VP1001, and the computer-based data management system are also described in Reference 18.

The mechanical and optical parts of the system comprise two separate modules, a TRANSMITTER, and a RECEIVER. The transmitter is a device for projecting a set of well-defined and controlled blue interference fringes into the test space. In the V-I configuration this is sufficient but in the full IMAX configuration the blue fringes must be surrounded by a green Gaussian spot of typically seven times the blue diameter. The receiver is an optical system that may be adjusted to have one photomultiplier observe only the blue light from the volume illuminated by the interference fringes and a second to collect only green light from a volume of about twice the projected area of the blue. The electrical signals and, hence, the information available from the light scattered by the droplet, is input to the composite V-I/IMAX INTERFACE BOX and thence to the VP 1001 electronic processor.

In the V-I mode frequency and contrast (visibility) are derived and translated into digital words by the VP 1001 processor whereas in the IMAX mode the size information is supplied from the V-I/IMAX INTERFACE BOX which contains intensity measuring circuitry in addition to photomultiplier voltage control and miscellaneous interfacing and housekeeping functions. The data are accepted by the data management

system (DMS) and may be displayed or reduced in a number of ways at the choice of the operator. Local floppy disc storage of reduced data sets is provided and the use and control is outlined under the DMS and software sections. Data may be printed.

Operator intervention is required for optical set-up and adjustment, choosing the correct processor and interface box settings and controlling the data manipulation via the DMS Keyboard.



Figure 5.0. Photograph of ADSS Optical System



Figure 5.1. Photograph of ADSS Electronics

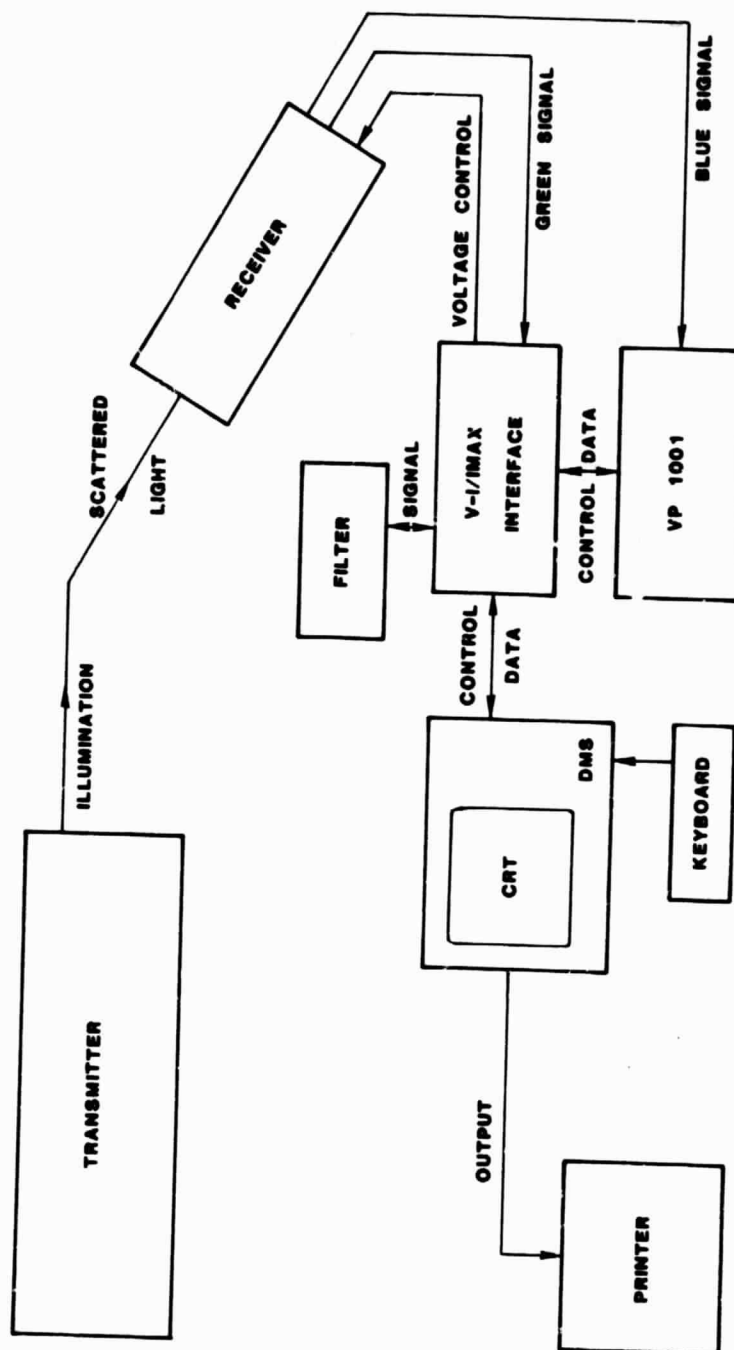


Figure 5.2. System Structure

5.1 Operating Ranges and Specifications

Droplet Size Measurable	5 μm to 1 mm
Doppler Frequency	2 KHz to 5 MHz
Fringe Spacing	3 μm to 65 μm
Sample Volume Diameter (Blue)	36 μm to 300 μm
	300 μm to 2.3 mm
(Green)	250 μm to 2.3 mm
Throw from Transmitter Face	583 mm to 820 mm
Output Beam Separation	4 mm to 110 mm
Laser Power (Argon Ion)	4 watts (nom)
(Blue)	> 1 watt at 514.5 nm
(Green)	> 1 watt at 488.0 nm
Polarization Ratio for each and both blue beams	Better than 100:1
Blue Beam Equality	Within better than 10%
Collection Lens	Focal length 610 mm. f/5
Photomultipliers	EMI 9781 B, S-5, Side Window
Narrow Band Filters	10 nm FWHM at 488.0 nm
	10 nm FWHM at 514.4 nm
Maximum Data Rate	8300/s in FAST mode 3800/s in NORMAL mode
Pinhole Sizes	50 μm , 100 μm , 200 μm 400 μm , 600 μm , 800 μm , and 1 mm

6.0 TRANSMITTER

This section is a brief overview of the design and some of the choices that have been made for this machine. It does not, in general, discuss the rationale behind these decisions. The machine is designed to operate in either the VISIBILITY-INTENSITY or the IMAX mode and many parts are common to both configurations. The main significant difference is that only in the IMAX configuration is a green beam required.

6.1 Transmitter Description

The function of the transmitter is to project two blue coherent laser beams and possibly one green laser beam into a chosen test space where there may be moving droplets. The droplets scatter blue light from the fringe pattern caused by the crossing beams and the frequency and modulation properties yield the velocity and size of the measured droplet in the VISIBILITY-INTENSITY configuration. In the IMAX configuration, the velocity is still derived from the fringe modulation frequency but the size is derived from the absolute intensity scattered from the green beam. The placement of the particle within the green beam is guaranteed by using the blue region as an exclusive condition. To optimize the fringe spacing and spot sizes adjustments are available in the transmitter. In general, it is necessary to perfect the new alignment each time anything is changed and these adjustments are simple.

Inside the transmitter's upper compartment there are movable components to change sample volume size by altering beam diameter, and number of fringes by altering beam spacing at the transmitter. The throw to the perfect waist is also changed if other parameters are to be held in their optimal range.

The first of these active components is a reversible zoom collimator to change the beam diameter by up to a factor of about 8, either as magnification or minification depending upon the orientation of the component. It is not focusable. The second adjustment is axial translation of one of two matched prisms to change the separation of the two beams. Between the two adjustable components is a path matched beamsplitter of fixed separation. Both of its output beams have small and precise angular adjustments to correct for any component errors which could cause the imperfect crossing of the two blue beams. When the IMAX mode is used there is also a green beam, separated from the blue by a dispersing prism, which may have its placement and diameter adjusted to suit the condition required.

The beamsplitter design is a fixed path-matched type using a nominally 50/50 splitter in S-polarization and there is provision for small alignments of the output beams to make the beams cross at the waist, whose distance from the transmitter varies somewhat with the beam size, an unfortunate but not catastrophic artifact of this otherwise simple and effective optical design.

The transmitter is a rigid aluminum enclosure of grooved and bolted construction which contains a Lexel Model Number 95-4, 4 watt Argon Ion Laser and various optical components to achieve the desired output properties. These are described in the following section.

Most alignments are available by removable of the top cover of the box. Other 'permanent' alignments may only be accessed by removal of one or more of the end covers. A knob at the rear of the enclosure operates the laser shutter to prevent radiation from being emitted from

the laser cavity even if power is supplied to the system. A red light at the rear of the transmitter enclosure indicates, regardless of the shutter position, that the laser is powered and potentially capable of emitting radiation.

Figure 6.1 identifies the principal transmitter components:

- A) Laser
- B) First Steering Mirror
- C) Dispersing Prism
- D) Second Steering Mirror
- E) First Green Steering Mirror
- F) Blue Color Selection Aperture
- G) Beam Diameter Control Telescope
- H) Beamsplitter Plate
- I) First Beamsplitter Mirror
- J) Second Beamsplitter Mirror
- K) Third Beamsplitter Mirror
- L) Fixed Separation Prism
- M) Movable Separation Prism
- N) Output Lens
- O) Second Green Steering Mirror
- P) Green Color Selection Aperture
- Q) Fixed Green Lens
- R) Zoom Green Lens
- S) Third Green Steering Mirror
- T) Fourth Green Steering Mirror
- U) Green Beam Stop

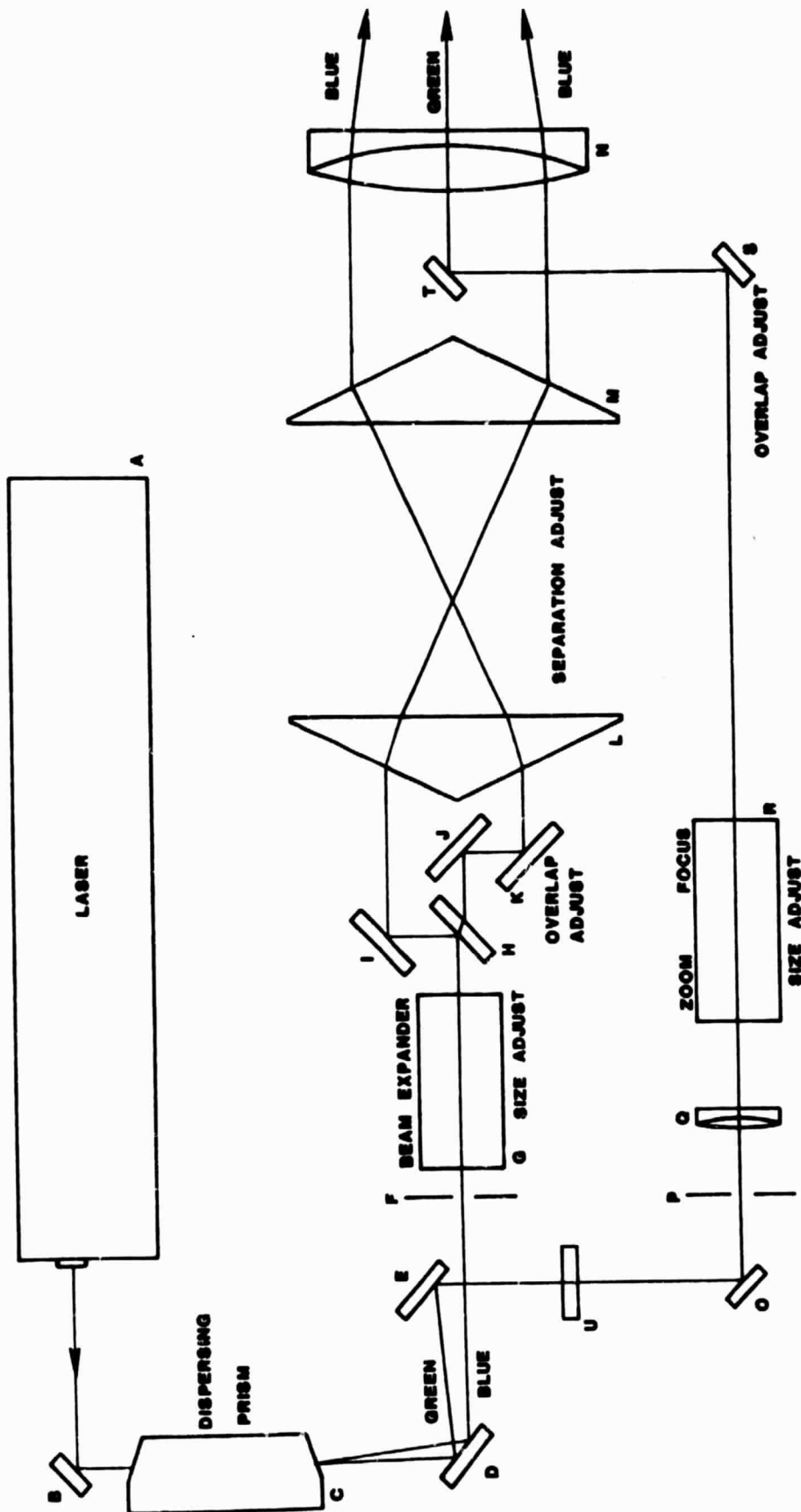


Figure 6.1. Transmitter Optics

7.0 RECEIVER

7.1 Receiver Description

The receiver is essentially a telescope with two photomultipliers to collect light from the focal point. It may be positioned to focus approximately onto the transmitted probe volume. External knobs offer fine tune pointing alignment and focusing of the entire assembly.

The receiver collects light that has been scattered from anything within the illuminated sample volume and directs it onto the cathodes of the photomultipliers. Each PMT collects light of one color only. The front lens assembly consists of a fixed front collimator lens of 125 mm diameter followed by an identical lens which may be axially translated to focus the system. Each lens has a focal length of approximately 610 mm. In correct alignment the light is focused onto two pinholes via a beamsplitter and mirror system. The beamsplitter is not dichroic and the color separation is achieved by narrow band filters internal to each PMT housing assembly. The pinholes are exchangeable but have no lateral movement. The entire receiver must be moved to correct misalignment. Lateral movement permits precise alignment with the image of a scatterer in the sample volume and axial movement of the inner front lens by the external focusing knob on the front face will permit precise focusing on the sampling volume provided that the distance from the sampling volume to the receiver is within the range of adjustment provided.

Within each PMT housing assembly is an optical system which images the receiver front aperture on the cathode of the photomultiplier. In the blue system there is also installed an intermediate aperture stop to control the 'collection factor.' In the section

between the two lenses that perform the above function, the light is almost collimated and it is here that the narrow band color selection filters are fitted. They reject light of anything but the chosen color for that PMT. Each of the identical PMT's is a side looking opaque cathode type and is robust but not indestructible.

Figure 7.1 identifies the significant components:

- A) Fixed Front Collecting Lens
- B) Focusable Inner Collecting Lens
- C) Fixed Beamsplitter
- D) Fixed Mirror
- E) Pinhole Carriers
- F) Collimating Lenses
- G) Aperture Stop (Blue System Only)
- H) Blue Narrow Band Filter
- I) Green Narrow Band Filter
- J) Final Lenses
- K) Fixed Mirrors
- L) Photomultiplier Tube

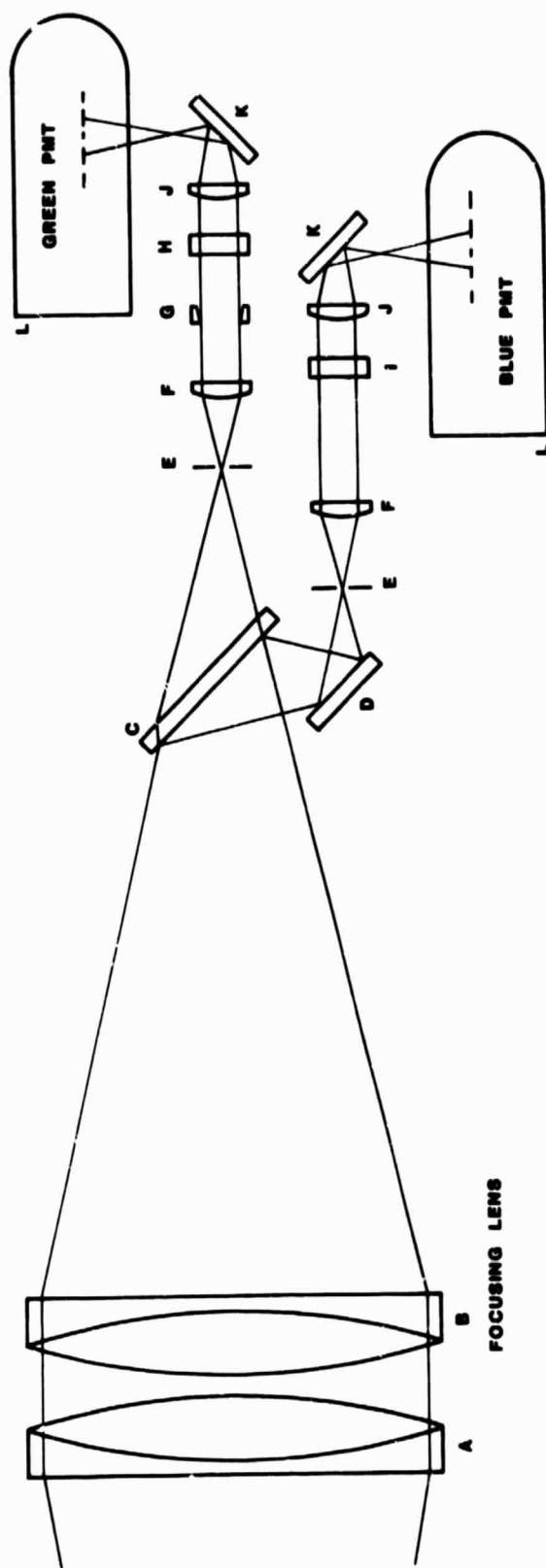


Figure 7.1. Receiver Optics

8.0 V-I/IMAX INTERFACE BOX

The V-I/IMAX INTERFACE BOX provides a central interface that enables the system to be operated in the V-I or IMAX modes without inconvenient electrical wiring connection changes. It is linked with the Receiver, VP 1001, DMS, and Krohn-Hite Filter boxes in a fixed configuration as illustrated on Fig 5.2. It performs the following functions in each of the operational modes according to the MODE switch setting:

- V-I a) HIGH VOLTAGE controls BLUE PMT.
(Requires H.V. DISPLAY set to BLUE PMT to show blue PMT voltage on VP 1001.
- b) All other functions are retained by VP 1001.
- c) Output word transmitted to DMS via this box.
- IMAX a) Measures intensity from the green beam and transmits this to DMS together with velocity data from VP 1001.
- b) HIGH VOLTAGE now controls GREEN PMT, blue control from VP 1001.

8.1 High Voltage Control

In the IMAX mode the high voltage for the blue beam PMT is controlled at the VP 1001 Processor while the green beam PMT high voltage is controlled at the V-I/IMAX INTERFACE BOX.

In the V-I mode the green beam PMT is inoperable and the blue beam PMT high voltage is controlled at the V-I INTERFACE BOX.

The high voltage control circuitry in the INTERFACE BOX is a more advanced version of that used in the VP 1001 Visibility Processor.

If the front panel switch of either unit is the MANUAL position then the high voltage is controlled by the front panel potentiometer from approximately 0 to 800 volts. If either switch is in the AUTO position, the high voltage is automatically controlled.

The criterion for automatic high voltage adjustment is that the amplitude (intensity) of signals in a selected visibility band shall have a given value. The visibility band from 47% to 53% has been chosen for both V-I and IMAX. The intensity band discriminator established six discrete intensity bands as shown below.

Intensity
X I_0

2.20	_____
	BAND 6
1.69	_____
	BAND 5
1.30	_____
	BAND 4
1.00	----Reference Level = 2.67 volts----
	BAND 3
0.769	_____
	BAND 2
0.591	_____
	BAND 1
0.455	_____

Each band has a counter to accumulate the number of valid data samples in that band with a visibility between 47-53%. The first one of the six counters to reach a count of eight causes all of the counters to be reset and also changes by one the count in the UP/DOWN counter that contains the 10 bit high voltage control word. The counters in bands 1, 2, and 3 increment the UP/DOWN counter and those in bands 4, 5, and 6 decrement the count. The LSB value of the control word corresponds to about 0.8 volts of high voltage.

When an equilibrium condition is established, the intensity value for 50% visibility should be very nearly equal to I_0 , corresponding to a signal voltage of about 2.67 volts. In the V-I mode the Gaussian intensity distribution of signals from randomly positioned droplets will yield a value higher than I_0 for particles in the center of the sample volume. The narrowness of the bands helps prevent bad data samples from influencing the setting. Six different bands are used so that the high voltage will 'pull-in' when the switch is changed from MANUAL to AUTO even if the manually set voltage was not very close to optimum.

8.2 Intensity Measurement

8.2.1 Overview

In the IMAX mode the peak intensity of the large green beam signal is measured and related to droplet size based on a square law relationship.

$$d = k \times I^{1/2}$$

where k is the constant of calibration determined from either known droplets or prior operational tests in the V-I mode. This theory is acceptable for droplet size ranges from 3 μm to 1 mm. In the V-I mode the size is determined from the visibility of the signal and the intensity is used merely to validate the individual readings based on an allowable intensity band which correlates with the individual visibility readings.

The intensity information to the V-I/IMAX INTERFACE BOX is derived from the LOW PASS FILTER MONITOR signal, from the VP 1001 when the V-I mode is operative, and from the GREEN PMT signal when in the IMAX state.

The signal from the LOW PASS FILTER MONITOR has a peak amplitude which exceeds 5 volts and must be attenuated (amplifier with a gain equal to 0.5) because the external low pass filter can handle signals of 4 volts maximum. The output signal from the green beam PMT (with amplifier within the tube assembly) should be one tenth of the low pass monitor signal and, hence, it is amplified by a factor of five so as to attain the same level at the external filter.

The external low pass filter is used to remove the high frequency noise from the pedestal signal. In the V-I mode, the filter also removes the Doppler signal from the pedestal. The filter is a Krohn-Hite Model #3200 and is used in its low pass mode only. The cut-off frequency should always be set at one-half of the lowest frequency on that range of the VP 1001 that is currently selected. For example, if the VP 1001 is set to range #1 the Doppler frequency may be between

2 and 5 MHz. Ideally the low pass filter must be set to 1 MHz. The back panel response switch should always be placed in the MAX FLAT position.

The output of the low pass filter is scaled by a X2 amplifier whose output is monitored by an offset nulling circuit. This circuit cancels offsets which arise from all previous unwanted circuit properties and stray background light. This circuit will hold the baseline of the signal between droplet events to zero volts so that the peak measurements have a constant correct reference. The peak detector is enabled only during the time of the LONG PULSE. The peak detector will capture and hold the peak value of the pedestal signal. The trailing edge of the LONG PULSE causes this analog value to be converted to a 10 bit intensity data word.

9.0 PUBLICATIONS

1. C.F. Hess, "A Technique Combining the Visibility of a Doppler Signal with the Peak Intensity of the Pedestal to Measure the Size and Velocity of Droplets in a Spray," AIAA Paper Number 84-0203, presented at AIAA 22nd Aerospace Sciences Meeting, January 9-12, 1984/Reno, Nevada.
2. C.F. Hess and V. Espinosa, "Spray Measurements with a Nonintrusive Optical Scattering Technique," 23(5), 604-609 (September/October 1984).
3. C.F. Hess, "A Nonintrusive Optical Single Particle Counter for Measuring the Size and Velocity of Droplets in a Spray," accepted for December issue of Applied Optics (1984).

REFERENCES

1. W.M. Farmer, Applied Optics, Vol. 11, No. 11, (1972).
2. D.M. Robinson and W.P. Chu, Applied Optics, Vol. 14, 2177 (1975).
3. R.T. Adrian and K.L. Orloff, Applied Optics, Vol. 16, No. 3 (1977).
4. D.W. Roberds, "Particle Sizing Using Laser Interferometry," Applied Optics, Vol. 16, No. 7 (1976).
5. W.D. Bachalo, Applied Optics, Vol. 19, No. 3 (1980).
6. J.D. Pendleton, Applied Optics, Vol. 21, No. 4. (1982).
7. M.L. Yeoman, B.J. Azopardi, H.J. White, C.J. Bates and P.J. Roberts, "Eng. Appl. of Laser Velocimetry" Winter Annual Meeting ASME. Phoenix, AZ, November 14-19 (1982).
8. A.J. Yule, N.A. Chigier, S. Atakan, and A. Ungut, J. Energy 1, 220-228 (1977).
9. D. Holve and S.A. Self, Appl. Opt. 18 (1979).
10. Y. Mizutani, H. Kodama and K. Miyasaka, Combustion and Flame 44:85-95 (1982).
11. A. Men', Y. Krimmerman, and D. Adler, J. Phys. E.:Sci. Instrum. 14 (1981).
12. P.R. Ereaud, A. Ungut, A.J. Yule, N. Chigier, Proceedings from "The 2nd International Conference of Liquid Atomization and Spray Systems," p. 261 (1982).
13. W.J. Glantschnig, M.W. Golay, S.H. Chen, and F.R. Best, Appl. Opt. 21 (1982).
14. B.H. Liu, R.N. Berglund, J.K. Argawal, Atmospheric Environment, Vol. 8, pp. 717-732 (1974).
15. H.C. van de Hulst, "Light Scattering by Small Particles" John Wiley and Sons, 1957, Chap. 12.
16. C.F. Hess, AIAA 22nd Aerospace Sciences Meeting, AIAA-84-0203 (1984).
17. D.W. Roberts, C.W. Brasier, and B.W. Bomar, Opt. Eng. 18 (1979).
18. Operator's Manual of the Advanced Droplet Sizing System, SDL No. 84-53020 (February 1984).